APPLICATION OF CONSUMER COLOR CAMERAS AS THREE-COLOR PYROMETERS

by

Megan Kimberly Tribble

Submitted in Partial Fulfillment

of the Requirements for the Degree of

Master of Science in Mechanical Engineering

with Specialization in Explosives Engineering

New Mexico Institute of Mining and Technology

Socorro, New Mexico

May 2014

ABSTRACT

A high-speed digital color camera was used as a three-color pyrometer to measure temperature fields in energetic material deflagration and detonation events. This measurement technique used the raw pixel intensity data recorded in the color images of high-speed events as a record of the radiant energy emitted in particular wavelength bands. By comparing the ratio of the radiation intensity in these different wavelength bands, the blackbody temperature of the radiating body was approximated. This temperature measurement technique was benchmarked against a spectrometer which recorded the spectral radiation distribution for the events studied. The initial calibration was performed by viewing a tungsten filament bulb. The high-speed camera was then used to record energetic material events including the deflagration of pyrotechnic mixtures of potassium chlorate and sucrose and the detonation of lead styphnate-based primer materials and NONEL shock tube. Overall, the results show that this technique can accurately measure temporally- and spatially-resolved temperature fields, which agree well with published values measured for similar deflagrations and detonations using other, more traditional techniques. This optical technique can potentially solve many issues associated with temperature measurement in high-speed events, especially in the explosives community. In addition to the temperature measurements made using the color camera, the spectrometer was used to measure the spectrum of light produced during these detonations and deflagrations. The measured spectra are important for other optical techniques, including schlieren and shadowgraphy, which would benefit from the use of illumination sources in wavelengths where low spectral energy is present in explosive events.

Keywords: pyrometry; temperature; radiation; color; explosives; pyrotechnics; spectrometry; high speed camera

ACKNOWLEDGMENTS

I would like to thank the numerous people who have supported, assisted, and encouraged me throughout my graduate studies. This includes Dr. Michael Hargather, who has been a wonderful research advisor and has guided me through my research these past two years with confidence and perseverence. Thank you to all of the members of the Shock and Gas Dynamics Lab (SGDL) who have helped me with testing, allowed me to tag along on their tests, and have been great, supportive friends. Thanks, in particular, to Melissa Candelaria-Lyons for preparing so many samples of pyrotechnics for me to image – your help was so greatly appreciated.

I'd also like to thank Lindsay Klennert, my manager at Sandia National Laboratories, as well as the Critical Skills Masters Program at Sandia for supporting my graduate studies financially and encouraging me to pursue my M.S. Innumerous people at Sandia have encouraged me and helped me academically, and I am grateful to each and every one of them.

My family has also been there for me through these past two years, especially during the most intensely difficult last few months. Vanessa Tribble–Mom– you are always there for me to tell you about my exciting adventures or cry on your shoulder when my world comes crashing down. Your constant praise, faith, and encouragement is my anchor in every storm and I hope to someday be the same for you. Daniel Diamond, I am so blessed to have you as my soulmate. It is difficult to remember my life before you, and I absolutely cannot wait to spend the rest of my life with you. I thank God for you daily.

Most importantly, I'd like to thank my Savior, Jesus Christ, for being there for me in my darkest of hours. You have loved me from the beginning of time and died for my sins because of Your love for me. I am eternally in Your debt and hope to know You more and more as I age. I can't wait to see the plans You have for me!

This thesis was typeset with LaTeX[1] by the author.

---

[1] The LaTeX macro package for the New Mexico Institute of Mining and Technology thesis format was written for the Tech Computer Center by John W. Shipman.

CONTENTS

LIST OF TABLES

LIST OF FIGURES

LIST OF ABBREVIATIONS

ADC	analog-to-digital converter
ANFO	ammonium nitrate fuel oil
B/G	blue-to-green intensity ratio
B/R	blue-to-red intensity ratio
CCD	charge-coupled device
CFA	color filter array
CMOS	complementary metal-oxide semiconductor
FWHM	full-width half-max
LCD	liquid crystal display
MSDS	material safety data sheet
NA	numerical aperture
NONEL	non-electric initiation tube
OH	hydroxyl group concentration
P/N	part number
R/G	red-to-green intensity ratio
RGB	red/green/blue
SDK	software development kit
SNR	signal-to-noise ratio
TLP	top left pixel
VPB	virtually-pivoted beam

This thesis is accepted on behalf of the faculty of the Institute by the following committee:

_____

Michael Hargather, Advisor

_____

_____

I release this document to the New Mexico Institute of Mining and Technology.

_____

Megan Kimberly Tribble   Date

CHAPTER 1

INTRODUCTION

Temperature measurement of energetic material events, such as explosions and rocket motor operation, can be a difficult task. Due to the immense energy released during the chemical reaction, temperatures can easily range from 1000-6000 K and occur within an extremely short amount of time. Engineers in the energetic materials field, nonetheless, need to accurately measure temperatures for many reasons, such as evaluating efficiency and design adequacy. This thesis aims to apply an existing relatively new technique to new test subjects and identify areas for improvement.

1.1   Temperature Measurement

Because temperature measurement is such a crucial capability, it is well-developed and widely-used throughout engineering disciplines. A myriad of unique temperature measurement tools exist, including thermocouples, thermometers, thermistors, integrated circuit temperature transducers, resistance temperature detectors, and infrared sensors. Each of these techniques possess its own characteristic advantages and applications. Despite the many techniques available, temperature measurement of energetic material events is still greatly limited in its capabilities. For example, the majority of these tools are unable to measure temperatures greater than 1573 K without limiting their useful life [1]. To illustrate this problem, Figure 1.1 compares the temperature measurement ranges for the four most common tools, and relates them to typical temperatures experienced in rocket and explosive testing.

In extremely high temperature applications, pyrometry is the most suitable method. Pyrometry, such as infrared measurement, is a form of temperature measurement that assesses an object's radiation without need for contacting the object of interest. By eliminating contact between the measurement device and the object, high-temperature-induced equipment failure can be avoided. This advantage can be clearly seen in Figure 1.1, as the pyrometric methods can process
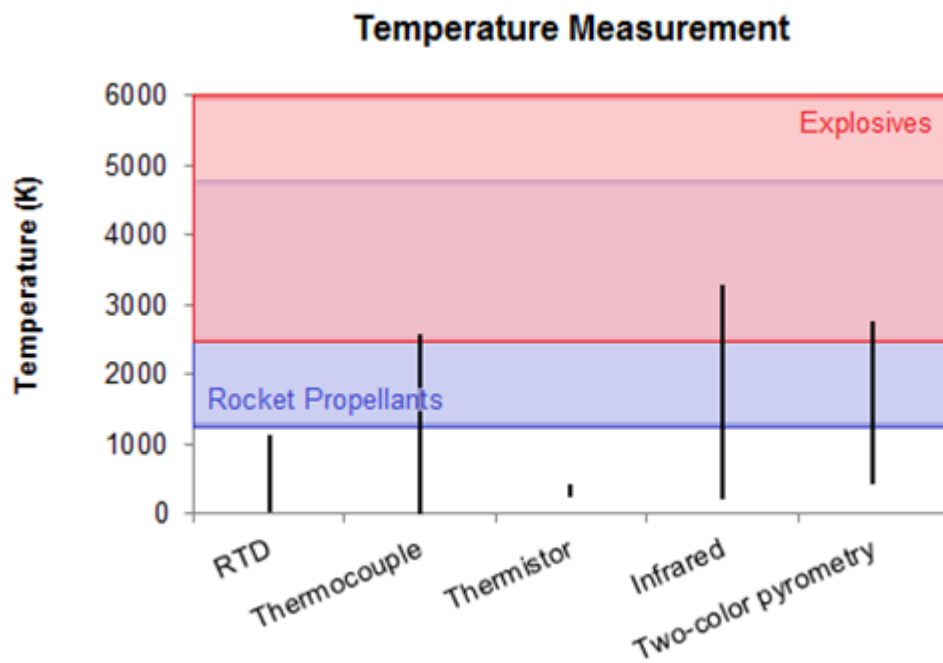
Figure 1.1: Common temperature measurement techniques and their working ranges. Note that the last two techniques are forms of pyrometry and can measure the highest temperatures.

the highest temperatures. While well-suited for high temperatures, infrared measurement is still lacking as it is costly and measures only one point at a time.

To be a truly useful temperature measurement technique for use with energetic materials, the following requirements must be met:

- Be able to withstand a destructive environment
  "...Any measurement system has to be able to withstand these high pressures [and temperatures] for sufficient time for the information to be transmitted to a data collection system before being destroyed. [2]"

- Have a quick response time
  "Typically, only techniques that involve the measurement of light emissions are fast enough to be able to track the short-lived, dynamic event[s associated with explosives] [3]" – ...this is because the response of light-emission sensors depends on the extremely fast speed of light [4].

- Be capable of measuring a large dynamic range
  Temperatures can range anywhere from 300 K (ambient temperature) to just under 6000 K.

- Measure temperatures with spatial resolution, rather than just one point measurement at a time
  Fireball temperatures are not the same throughout the fireball–for the least complex fireball, a gradual variation exists from the highest temperatures at the core to the lowest temperatures at the outer edges. Rocket motors are much more complex in that the combustion products are forced through a nozzle resulting in complicated fluid dynamics and temperature concentrations.

1.1.1   High-Temperature Measurement Applications

In some fields, the measurement capabilities are sorely inadequate for the range of temperatures experienced during testing. In explosive testing, for example, one group of researchers [4] was forced to use thin metal gauges to measure temperature. To acquire useful data, a detectable change in the data had to be measured before the gauge was destroyed. This delicate operation is not only time-consuming, as the gauge had to be replaced after every shot, but also costly.

Rocket testing can also be extremely damaging to metric equipment. Rocket motors produce thrust through the rapid expulsion of high-temperature combustion products through a nozzle. These combustion products can range from

2773K to 4673K for liquid fuel, and 1273K to 3373K for solid fuel, making temperature measurement a challenging task [5]. A reliable pyrometry method for these high temperature fields would be an invaluable addition to the engineer's toolbox.

1.2 Thermal Radiation: Color and Light

All objects emit thermal radiation, which is the fastest heat transfer mechanism out of the three types–conduction, convection, and radiation. The small portion of thermal radiation that the human eye can recognize (wavelengths of 400 - 760 nm) is perceived as light and color.

To fully realize the maximum radiation of an object at a given temperature, the theoretical concept of a blackbody was developed. A blackbody is a perfect emitter (optimal and uniform energy emission in all directions) and perfect absorber (all radiation is absorbed, regardless of wavelength or direction) of radiation. In 1879, Joseph Stefan determined that the radiation energy E_b emitted by a blackbody per unit time and per unit surface area is

$$E_b(T) = \sigma T^4, \text{ where } \sigma = 5.670 \times 10^{-8} \, {}^W/_{m^2 \cdot K^4} \qquad (1.1)$$

The radiation energy is directly proportional to the fourth power of the temperature [6], which explains why an extremely hot object will begin emitting a detectable amount of visible radiation (a glowing color.) This relationship between visible radiation and temperature is the reasoning behind the proposed research. By studying the color intensities of a high-temperature object, it is hypothesized that the object's temperature can be determined.

1.2.1 Theoretical Predictions of Blackbody Radiation

Using the related Planck's Law (discussed in detail in Section 5.5), the blackbody emissive power as a function of wavelength and temperature can be calculated, as shown in Figure 1.2. Only objects in the range of about 1000-6000 K produce radiation visible to the human eye. Objects at less than 1000 K radiate mostly in the infrared spectrum, and hence are only visible to the human eye through the reflection of light originating from other objects, such as light sources.

Pyrometry uses the relative intensities of various wavelength bands to measure temperature. Using the emissive power from Planck's Law, the relative
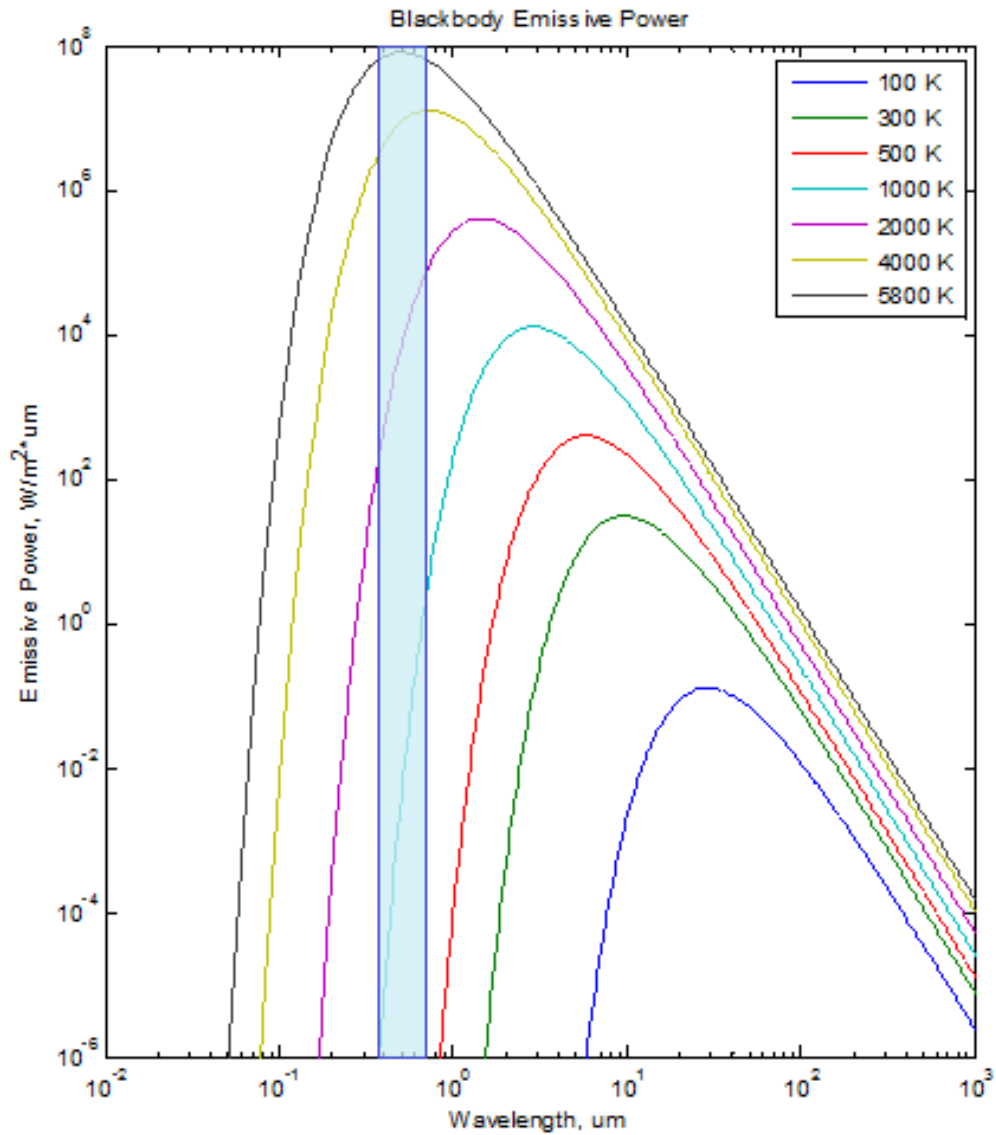
Figure 1.2: Blackbody emissive power as a function of wavelength and temperature. Note that the peak power at 5800 K is centered in the visible spectrum which is indicated with blue shading.)

intensity ratios across the red, green, and blue wavelength-bands for a blackbody can be calculated for each temperature, a plot of which is shown in Figure 1.3. The selection of the boundaries for the red, green, and blue wavelength bands is discussed in Section 3.2. This plot shows the theoretical color ratios that will be measured with the digital cameras later in this thesis. The unique trends of each color ratio will provide the basis for calculating temperature.

Figure 1.3: Red-to-green, blue-to-green, and blue-to-red color ratios for a blackbody as a function of temperature as calculated from Planck's Law.

1.3   RGB Color Optics in Cameras

Digital color cameras do not have sensors that detect individual colors. The CCD and CMOS sensors are sensitive only to light in general, with no wavelength preference. To yield color images, color filters are attached to individual pixels in the pixel array, thus effectively converting the all-light sensitive pixels

6

into individual color receptors. For all intensive purposes, all digital color cameras use red, green, and blue filters to replicate normal human vision [7]. The sensors respond to the incoming filtered light, measuring the proportions of red, green, and blue present in the scene. Each pixel's response to the filtered light is then "demosaicked" by the camera's algorithm to reproduce the scene that the human eye sees.

The red, green, and blue filters are most commonly arranged in a specific pattern known as the Bayer filter pattern [8], shown in Figure 1.4. The Bayer filter, designed and patented by Bruce Bayer in 1976, uses twice as many green filters as red and blue ones to mimic "the human eye's tendency to see green luminance as the strongest influence in defining image quality [9]." As light impinges on the Bayer filter, each pixel filters the light by its spectrum of wavelengths. If a wavelength corresponding to red exists in the impacting light, the light will transmit through the red filters. Similarly, green-wavelength light will transmit through the green filters, and blue-wavelength light will transmit through blue filters.
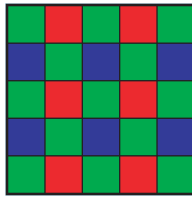
Figure 1.4: The Bayer filter pattern.

The unprocessed (raw) image is a mosaic of poorly-defined boundaries, and must be "demosaicked" to produce a clearer image. In this process, the color for each pixel is interpolated using the surrounding RGB values, resulting in an image that replicates the physical scene. In this research, demosaicking is undesirable as it modifies the true sensor readings. To avoid demosaicking, the unmodified pixel data is acquired in the form of raw images and video. By using the wavelength-specific light sensing capabilities of digital color cameras, a new radiant-energy temperature measurement technique is proposed for measuring extremely high temperatures.

1.4   Objectives of Present Research

The goal of the present research is continue the work of Densmore et. al (discussed in Section 2.4) by developing a unique temperature measurement tool well-suited for the extremely high temperatures present in explosive products.

From the review of prior research related to extremely high temperature measurement (Section 2), it is clear that there is a need for a non-contact-based technique in areas such as explosive and rocket motor testing. Current techniques easily fail due to the destructiveness of these events, can be costly, and do not always possess fast enough response times. Using the RGB data from consumer digital color cameras will answer the need for an accurate, low-cost, long-life tool. In addition, use of this technique with various new test subjects will both expand the library of this technique's applications, as well as provide temporally- and spatially-resolved temperature information not previously measured for various objects and energetic materials.

CHAPTER 2

LITERATURE REVIEW

2.1 Introduction

Prior to testing the red/green/blue (RGB) temperature measurement technique, previous research in two main areas will be discussed. First, techniques currently available for extremely high temperature measurement will be presented, as well as each technique's advantages and disadvantages. Second, research in which RGB color data was used to analyze experimental results will be mentioned. Successes and failures reported from this research will also be discussed.

2.2 Current Methods for Extremely High Temperature Measurement

There are many temperature measurement tools available for use in scientific experiments. These tools include thermometers, thermocouples, infrared pyrometers, thermistors, integrated circuit temperature transducers, and resistance temperature detectors. For extremely high temperature applications (greater than 1573K), however, there is a dearth of accurate, low-cost, long-life tools. Currently, the most cost-effective and widespread temperature measurement techniques are contact-based. The term "contact-based" means that the temperature probe must be in contact with or very near the subject material in order to measure its temperature. This close proximity to the heat source frequently limits the useful life of the temperature probe. In many cases, the measurement tool must be regularly serviced or replaced because it is poorly suited for such high temperatures. As researchers continuously aim to keep experimentation costs down, they have developed alternative temperature measurement methods, many of which are not contact-based. These alternative methods will be discussed in the following sections.

2.2.1 Explosives

Knowing the temperature of an explosive detonation product is important to understanding the performance of the explosive compound [4]. Smilowitz et al. observed the thermal explosion temperatures associated with PBX-9501 using K type thermocouples, which are accurate to ± 9K but are slow with response times ranging from 1.5 to 10 ms [10]. The fireballs produced by explosives can contain extreme temperatures as high as 5500K [11], instantly obliterating contact-based temperature measurement devices. A few techniques have been developed to counter the contact-based issue. Lewis and Rumchik measured the apparent temperature of post-detonation fireballs using atomic emission spectroscopy [12]. They found that their measured temperature agreed well with the theoretical calculation of 3000K. Cavanough and Onederra developed an instrumentation system for measuring the temperature of low density (low shock) commercial explosive events [4]. This system used thin film metal gauges which, due to their low mass, can detect a temperature change during the short shock pulse. To acquire the desired data, a detectable change in the data had to be measured before the gauge was destroyed by the blast–a delicate operation. Unfortunately, the team's use of a contact-based measurement tool also required that they replace the destroyed component after each shot. By requiring time and resources to replace damaged components after each shot, the experiment was made less efficient and more costly.

2.2.2 Rocket Motors

In rocket motor testing and application, temperature measurement plays a key role in understanding the motor's performance. A high combustion temperature translates to a high chemical energy content per propellant unit mass [5]. This chemical energy content is one of the most common performance metrics used in evaluating all types of rocket motors. Therefore, accurately measuring combustion temperature is a capability greatly desired by the rocket engineer. Because rocket motor combustion products are at such high temperatures (2500K to 3600K for common propellants [5]), a non-contact-based measurement tool is the best option.

To combat the contact-based measurement problem, alternative temperature measurement techniques have been researched and developed. No-contact techniques are radiation based, whether using visible radiation (color) or the invisible parts of the spectrum. For example, Wehrmeyer et al. successfully employed single-pulse laser ultraviolet and visible Raman spectroscopy to measure temperature for rocket motor injector development [13]. Unfortunately, this

technique relied upon the availability of an independent pressure measurement which can vary spatially throughout the chamber. Later development showed that a similar technique is applicable specifically to hydrogen at moderate pressures without the need for pressure measurement. Still, this measurement method only collects data at a point, whereas it is often desirable to measure the temperature of the entire chamber (two dimensions).

Strand et al. used–often costly–IR pyrometers to study hybrid rocket gas and fuel surface temperatures [14]. Chiaverini utilized embedded 25μm thermocouples to measure the surface temperature of a rocket's propellant [15]. This technique, however, required that the thermocouples be embedded in the propellant during casting, which does not allow for a quick change in measurement location, and only measures one point in the propellant block.

2.3 Utilization of Digital Cameras in Scientific Fields

Since the advent of digital cameras, researchers have exploited digital data for many different scientific purposes. Because they can deliver data directly in raw RGB format, digital cameras, including high-speed cameras, are well-suited for measurement of various properties. As an example, Hargather used the green plane of RGB color data to detect shockwaves during explosive events [16]. By collecting image and video data in raw format, the digital image processing pipeline can be avoided, reducing measurement difficulty. In addition to delivering raw data, digital cameras are often less costly than current measurement equipment and more widely available, making them prime for use during experimentation.

2.4 High Temperature Measurement

The RGB color model has also been researched previously as a high temperature measurement tool, but for comparatively lower temperatures than currently proposed. Fu et al. used a color charge-coupled device (i.e. a color camera) to measure diesel engine combustion temperatures of 1882K [17]. This technique was compared with the accurate results of a fiber-optic-spectrometer, and a difference in measurement of only 138 K was found. Tarasov et al. filtered the light from PETN explosions at 487 and 678 nm using the two-color pyrometry concept [18]. Lebel et al. note that fireballs have limited optical depth, therefore, only outer shell temperatures can be measured using radiation-based techniques [3]. In a review of temperature measurement techniques, Childs et al. describe two-color temperature measurement (an RGB technique variation) as very fast,

applicable from 423K to 2773K (source: 150 to 2500 °C), and accurate to within $\pm$10K. Unfortunately, Childs et al. note that the two color technique is currently very costly and not commercially available [19].

The additional wavelength used in three-color (RGB) pyrometry eliminates the need to calibrate the system when a change in geometry occurs [17]. In addition, by relying on the RGB color model, commonplace RGB-based digital and high-speed cameras can be exploited as pyrometers. Using the three-color pyrometry concept, Panditrao and Rege used a consumer-grade digital camera to accurately calculate the temperature in a furnace [20]. Their results were highly accurate when compared with the usual contact-based measurement method–an error range of 5% was listed in one paper [21]. To calculate the temperature, images of a flame were decomposed into their RGB components. These components were then compared to a calibrated histogram representing the range of values in the image. From this data, the temperature of the flame was interpolated. This research was performed on a furnace operating from 873K to 1273K (source: 600-1000 °C.)

More akin to the research discussed in this thesis, Densmore et al. successfully used a high-speed color camera to measure the more extreme temperature of Composition C-4 explosions [22]. It was noted, however, that extra care should be taken when measuring large temperature range events and metalized explosives. In addition, the authors remind the reader that, because the fireballs are optically thick, the temperatures measured are those present near the surface of the fireball's spherical shape. While the research presented here follows that of Densmore et. al, there are a few differences. First, only raw data is collected from the events in order to avoid modifying the true sensor response. Digital image processing adds complicated variables into the measurement technique, increasing the chances for error and poor results. Second, a spectrometer is used during testing not only to watch for problematic spectral features, but also to measure temperature using other proven methods. This research aims to apply the technique developed by Densmore et. al to new test subjects, as well as identify areas for improvement.

CHAPTER 3

EXPERIMENTAL EQUIPMENT

3.1 Spectrometer

To select the appropriate spectrometer, an in-depth comparison among available spectrometers, as well as their respective capabilities, was performed. This comparison focused mainly on spectral range, cost, resolution, charge-coupled device (CCD) pixel count, analog-to-digital converter (ADC) bit depth, integration time, and the signal-to-noise ratio (SNR.) Similarly, the spectrometer was selected based on similarities with those used by other sources mentioned earlier.
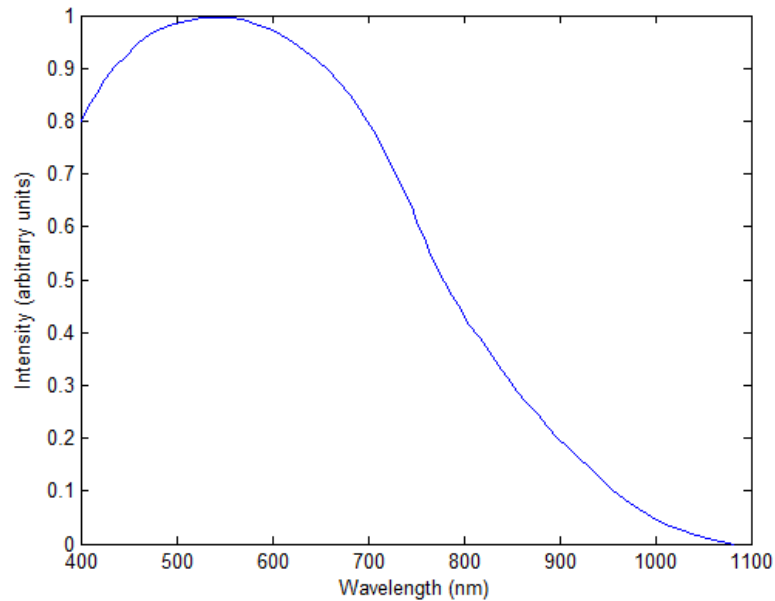
Figure 3.1: Spectral response of the CCD used in the Thorlabs CCS200 spectrometer at room temperature.[23]

The Thorlabs CCS200 spectrometer was selected due its low cost to wavelength range ratio, as well as its high pixel count and integration time range.

Some of the most important specifications are shown in Table 3.1. In addition, the spectral response of the spectrometer's CCD is shown in Figure 3.1–this data was used to calibrate the spectrometer for temperature measurement.

Figure 3.2: Thorlabs CCS200 spectrometer with cosine corrector installed on the fiber end.

During the first few experiments, the standard manufacturer-provided 200 μm core size, 0.22 NA, high OH, 1 m-long fiber (Thorlabs P/N M0065-51-0034) was used. Thorlabs also offers a cosine corrector (shown in Figure 3.2) for use during free-space measurements, such as a flame or fireball. The cosine corrector uses a diffuser to collect light from a 180° angle with respect to the diffuser surface. Since the diffuser is 0.5 mm thick, it induces a large intensity loss. According to Thorlabs, it transmits 0.2% at 660 nm. As such, the effect of the cosine corrector was not studied until later flame tests were performed.

Table 3.1: Thorlabs CCS200 specifications.

Wavelength Range	200-1000 nm
Spectral Resolution	<2 nm at 633 nm
Integration Time	10μ- 60 seconds
CCD Pixel Count	3648
ADC Bit Depth	16
Cost	$2,750

One of the most effective methods to control the spectrometer's light collection is the integration time, which can be changed by the user instantly. The integration time is the time duration that the spectrometer collects a spectrum–effectively, it's exposure time. A longer duration integration time will result in higher spectral intensities–both from the subject and the surroundings. This

value, as well as the fiber core size, were optimized for each test in order to collect high intensity spectra while avoiding sensor saturation in the spectrometer.

3.2   High Speed Cameras

Three high-speed color cameras were used during the energetic material tests–a Phantom v611 (primers), v710 (pyrotechnics), and v7.1 (NONEL); these cameras are shown in Figure 3.3 for comparison. Table 3.2 shows the properties of these high-speed cameras manufactured by Vision Research.

Figure 3.3: The three Phantom cameras used in this research. *Left to right:* Model v611, v710, and v7.1.

Table 3.2: High-speed camera specifications.

Camera Model	v611	v710	v7.1
Maximum Frame Rate (fps)	680,000	680,000	10,000
Sensor Format	CMOS	CMOS	CMOS
Pixel Count (Mpx)	1.024	1.024	0.480

The extremely high frame rate capabilities of these cameras–and those like them–make them well-suited for imaging explosions. In addition, the spectral response of the v611 and v710, shown in Figure 3.4, is published by Vision Research, simplifying the necessary calibration process discussed in Section 5.5. Due to the age of the v7.1, no spectral response data is available from Vision Research. As mentioned in Chapter 5, the sensors in all three of these cameras are overlaid with a traditional Bayer filter pattern which was confirmed by viewing red and green lasers.
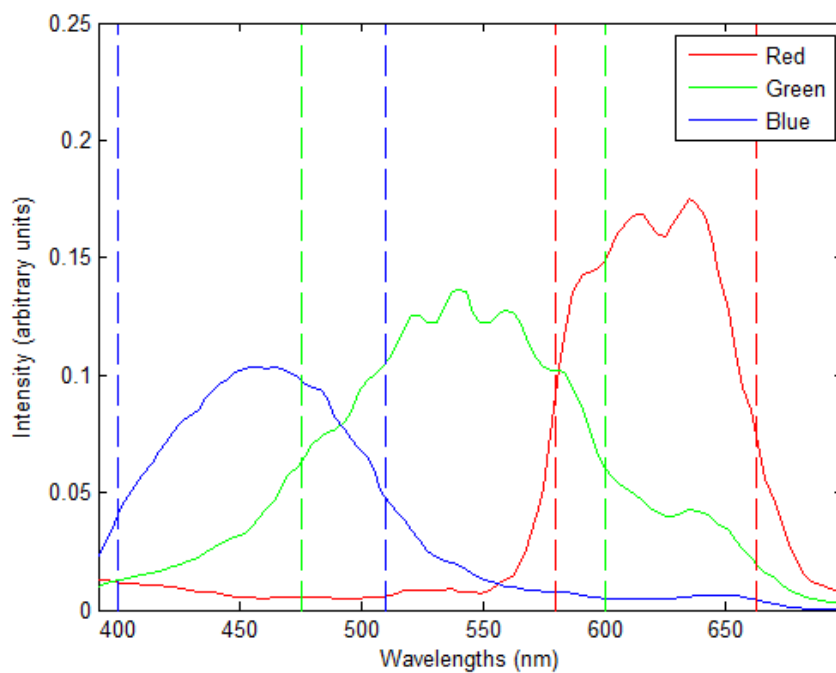
Figure 3.4: Spectral response of the Phantom v611 and v710 sensors published by Vision Research [24]. Full-width half-max (FWHM) wavelength bands identified with dotted lines.

CHAPTER 4

SPECTROMETRY

The proposed three-color technique is fundamentally based on the concept of two-color pyrometry–therefore, spectrum measurements are a crucial aspect of calibration and testing. Spectra provide calculated temperatures with which the three-color method can be compared, allow the blackbody characteristics of the subject material to be determined, as well as indicate the presence of emission that might affect results.

4.1 Benchmarking the Spectrometer

Prior to using the CCS200 spectrometer for data collection, several tests were performed to check its calibration and resolution. The simplest test consisted of viewing red and green lasers through the fiber. During this portion of testing, a handheld <5 mW green laser pointer and a higher-powered laser were evaluated. In addition, the overall spectrometer calibration and resolution capabilities were checked with a xenon bulb and a sodium-burning candle flame, respectively.

In Figure 4.1, the green laser's spectrum shows a peak at 532 nm which matches the published wavelength for green. The lower-intensity infrared peak at approximately 808 nm is attributed to the process used to produce light at 532 nm. According to Galang et al., a laser diode initially generates light at a wavelength of 808 nm [25]. By focusing this light onto a neodymium crystal, the light is converted to a wavelength of 1064 nm. Last, a frequency doubling crystal emits the light at a wavelength of 532 nm. Good quality green lasers have a filter to remove most, but not all, of the infrared components of the light, therefore the peak at 808 nm is much smaller than the 532 nm peak.

The results from a high-powered Lansing Research Corporation virtually-pivoted beam (VPB) red laser (Model 35.102) are also shown in Figure 4.1. The peak at 632 nm matches the published wavelength for red helium-neon laser illumination.

The last calibration check performed on the CCS200 spectrometer was to determine the resolution of the instrument using sodium. It is well known that the sodium spectrum is dominated by the intense doublet known as the Sodium D-lines at 589.0 and 589.6 nm [26]. To determine if the spectrometer was capable of such a high resolution, the spectrum of a candle flame was imaged as table salt was sprinkled into it. Figure 4.2 shows the background-corrected candle flame spectrum with the peaks of the sodium D-lines visible. The CCS200 easily meets its resolution specification of <2 nm.
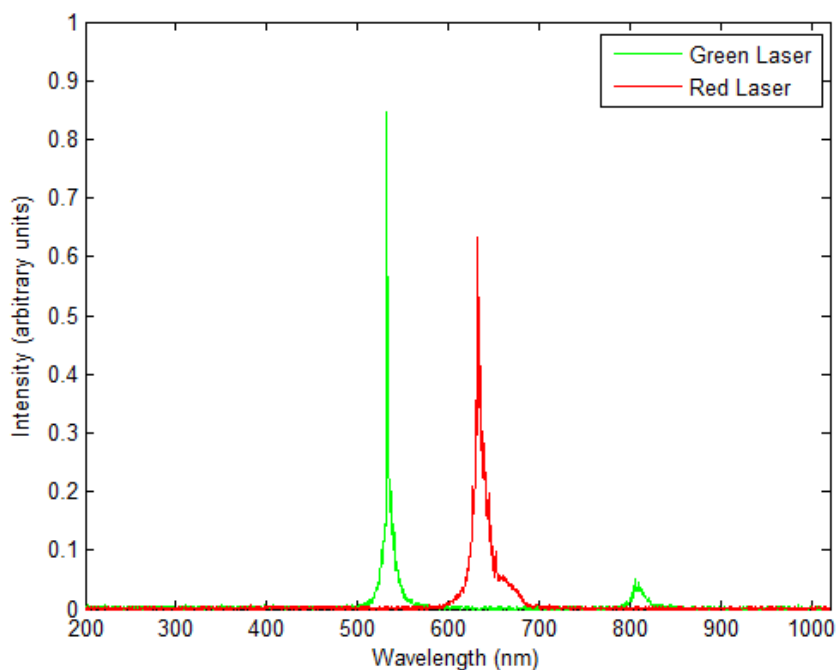
Figure 4.1: Green (0.3 ms integration time) and red (0.01 ms integration time) laser spectra.

4.2 Spectra of Various Light Sources and Energetic Materials

As mentioned at the beginning of this chapter, spectra were collected simultaneously with image and video data to perform several functions, one of which is to observe any significant emissions that will alter the calculated temperatures. The following sections show examples of the spectra for various subjects.
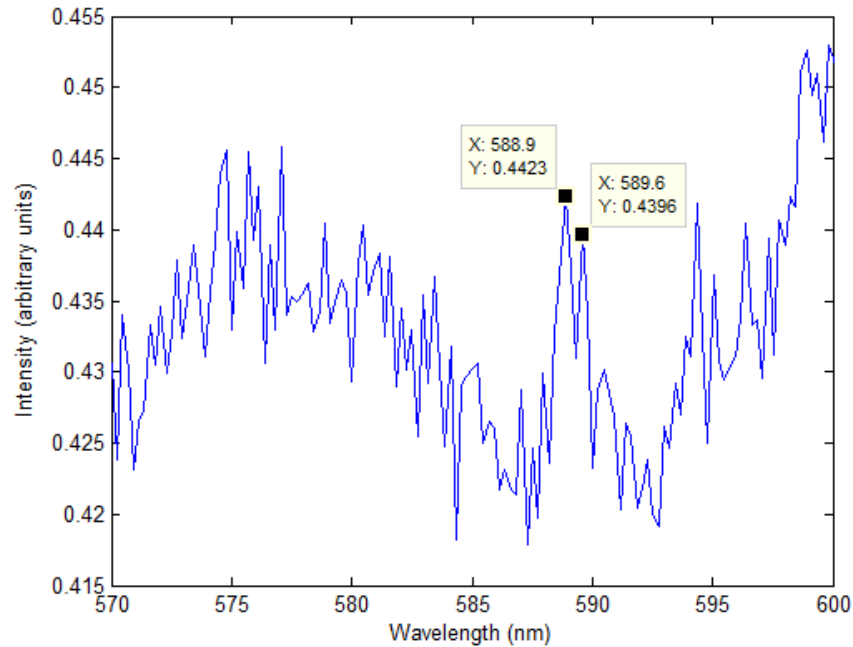
Figure 4.2: Spectrum of a candle flame showing the sodium doublet peaks (100ms integration time.)

4.2.1 Light Sources

The spectrum of a high-intensity Newport arc lamp (Model 66921 using bulb P/N 6271), which can be used for illumination in Schlieren optical techniques, was measured with the spectrometer. The complex spectrum, shown in Figures 4.3 and 4.4, exhibits significant visible radiation, as well as higher-intensity spectral peaks in the infrared region. Its spectrum was compared with the published spectrum from Newport Corporation [27]. The published chart was processed using the Graph Suchi Yomitori System to obtain physical data points [28] and compared with the observed spectrum; the comparison is shown in Figures 4.3 and 4.4. While this comparison does not, by itself, prove calibration of the spectrometer, it does show that the measured spectrum agrees well with the published values in the 800-1000 nm range.
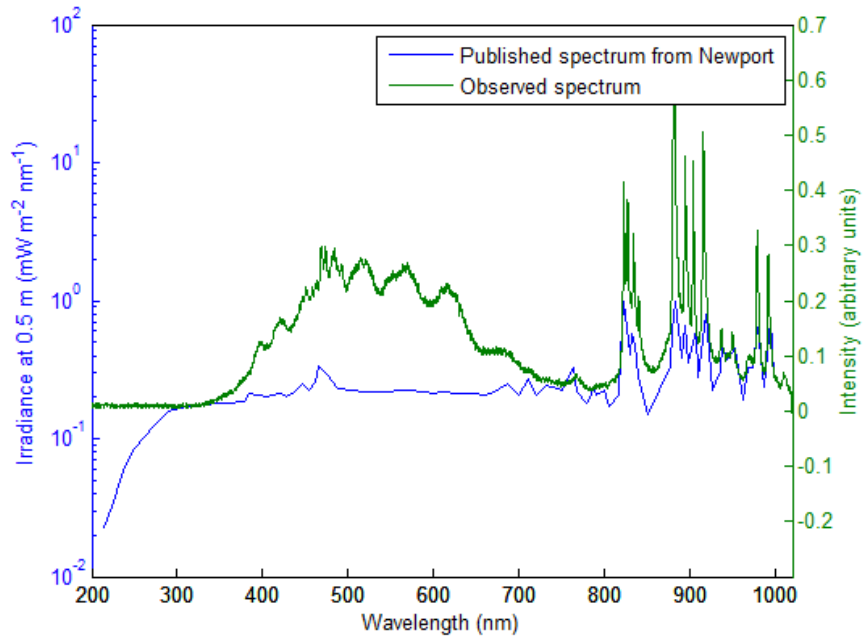
Figure 4.3: Xenon spectrum with an integration time of 0.15 ms (green) compared to the published Newport values (blue.)
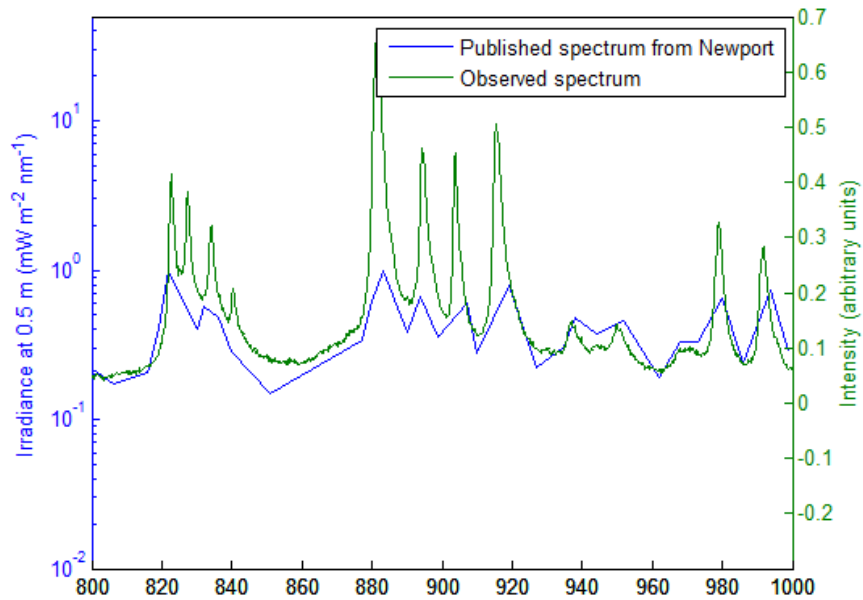
Figure 4.4: Spectra comparison in the 800-1000 nm range. Roughness present in the published spectrum is due to the graph-to-data-point conversion process.

In addition to studying the arc lamp's spectrum, the spectrum of the tungsten-filament bulb used later in this research to calibrate the three-color pyrometry system was also measured with the spectrometer. It's spectrum showed higher intensities in the visible region, as well as high levels of infrared radiation.
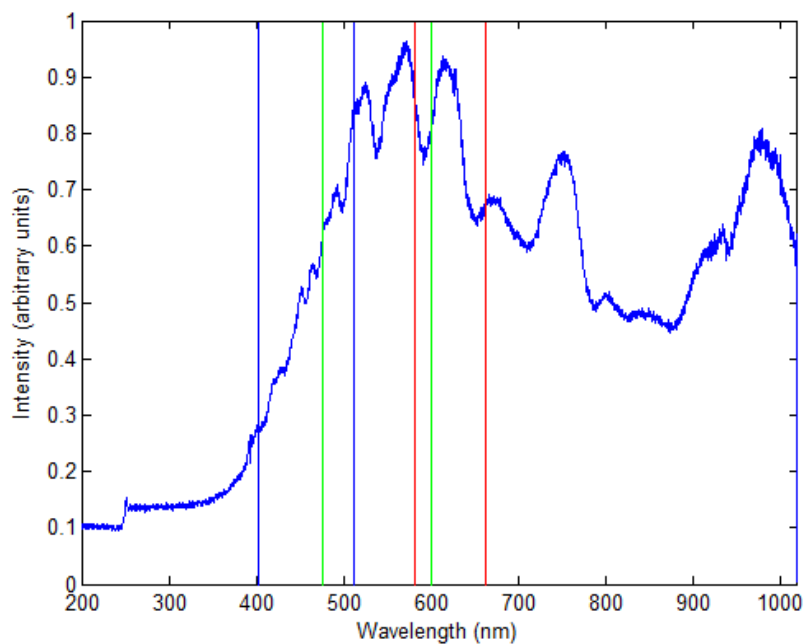
Figure 4.5: Spectrum of the tungsten bulb used for calibration (17 ms integration time.) The red, green, and blue wavelength bands selected based on the Phantom V611's FWHM are shown.

4.2.2 Shotgun Shell Primers

Available from most firearms or hunting equipment suppliers, Remington 209 Premier STS shotgun shell primers were fired approximately 5 cm away from the fiber end, which was aimed at the center of the primer face and at a slightly offset angle so as not to obstruct the simultaneous high-speed video being collected head-on. Figure 4.6 shows an example of the spectrum measured from a shotgun shell primer.
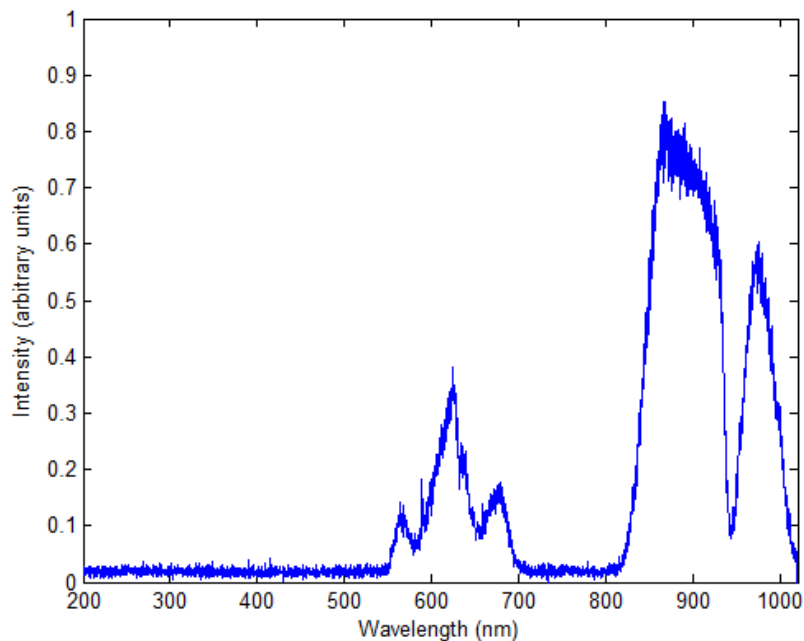
Figure 4.6: Spectrum of a shotgun shell primer (integration time of 500ms.) The presence of large-amplitude noise is due to the high integration time used.

4.2.3 Pyrotechnic Mixture

A common pyrotechnic mixture, a combination of potassium chlorate ($KClO_3$) and sucrose (table sugar–$C_{12}H_{22}O_{11}$), was imaged with the spectrometer, as well. This mixture was prepared with the amounts necessary for oxygen balance, which optimizes heat output. Figure 4.7 shows the spectrum collected for this mixture. The most notable feature of this spectrum is the large peak at 768.5 nm. This peak, located just past the visible spectrum on the infrared end, agrees with the pink light visible during deflagration.
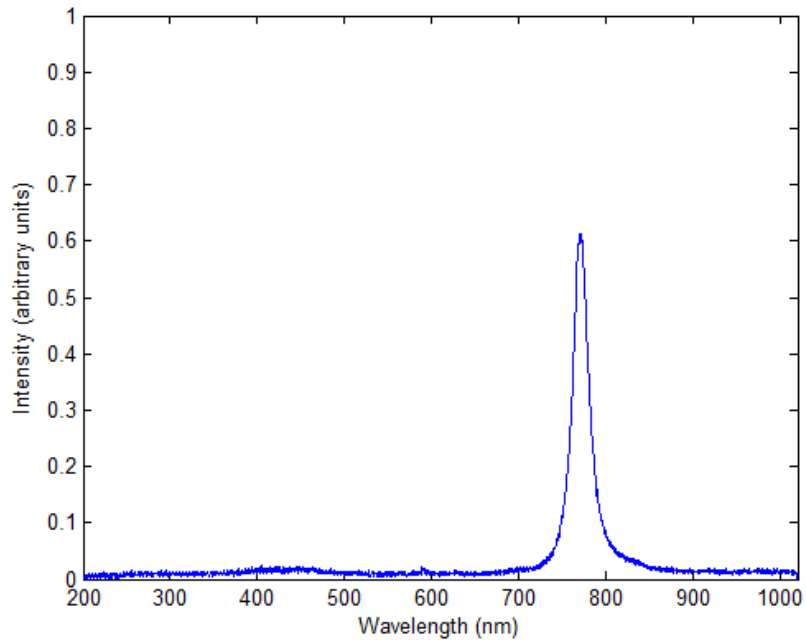
Figure 4.7: Spectrum of a common pyrotechnic mixture (potassium chlorate and sucrose) prepared at the oxygen balance viewed with an integration time of 6 ms.

4.2.4   NONEL

NONEL lead line is a non-electric shock tube initiation system designed by Per Anders Persson at Nitro Nobel in 1973 [29]. It is comprised of a three-layer plastic tube, the innermost surface of which is thinly coated with the explosive mixture of HMX and aluminum. This shock tube is widely used for initiation of various explosive trains. Figure 4.8 shows a sampling of the NONEL spectrum. Due to the high propagation rate of NONEL and difficulties with triggering the spectrometer, the highest intensity spectrum only reached a maximum amplitude of 0.03. With a spectrometer with more reliable triggering capabilities, spectrum measurement can be improved. The following plot serves to show the general shape of the spectrum for NONEL.
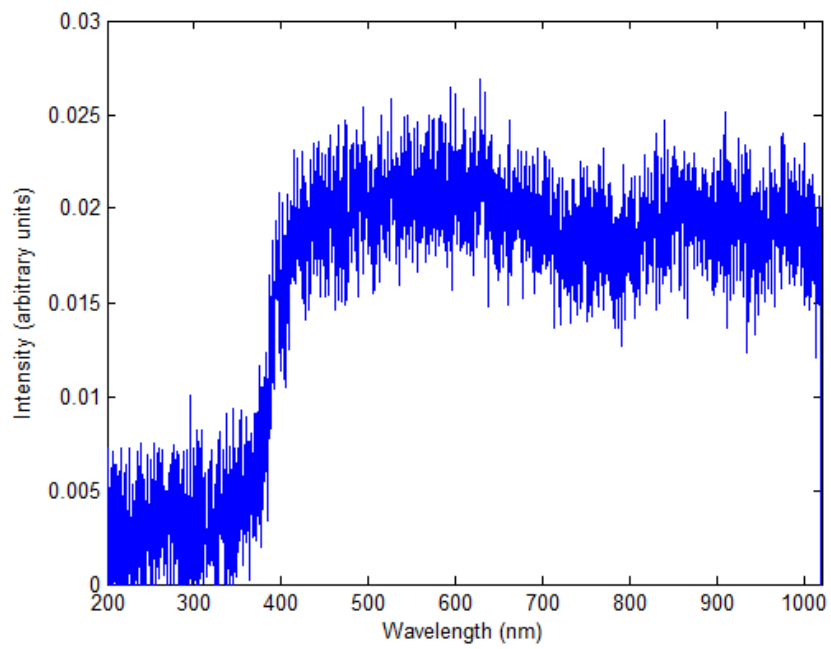
Figure 4.8: Spectrum of NONEL lead line at an integration time of 200 ms.

CHAPTER 5

ANALYSIS PROCEDURES AND MATLAB CODE EXPLANATION

To ensure repeatability, improve speed, and maintain quality of the temperature calculations in this research, data processing was performed using MATLAB code. The full code developed for this research is located in the appendices, while this chapter discusses, in detail, the approach taken and methods used in each set of code.

5.1 Blackbody Calibration

Before attempting to measure temperature with the three-color technique, the Pasco Scientific TD-8555 tungsten-filament Stefan-Boltzmann lamp was imaged with the system. During this calibration, the lamp, which functions as an approximate blackbody, was viewed simultaneously with the high-speed Vision Research Phantom v611 and the Thorlabs CCS200 spectrometer (all of which are shown in Figure 5.1) at six different power levels ranging from 6.5-11.5 V in approximately 1 V increments. This data was taken without ambient lighting present and no cosine corrector was used. The effects of these two variables are discussed in further detail in Section 5.1.3. The resulting intensity data was then related to the theoretical temperature of the filament to compare the sensitivities of the various devices.

Tungsten filaments are frequently used to calibrate two-color pyrometry system, an example of which can be found in [20]. This is because tungsten-filament bulbs emit light solely due to the filament's temperature and because the filament's resistance during operation can easily be used to determine filament temperature, as shown in Figure 5.2. The voltage and current values displayed on the lamp's power supply were used to determine lamp resistance. The relative resistances with respect to the ambient resistance of 0.5Ω were used in conjunction with the curve fit equation displayed in Figure 5.2 to determine the theoretical temperatures of this blackbody.
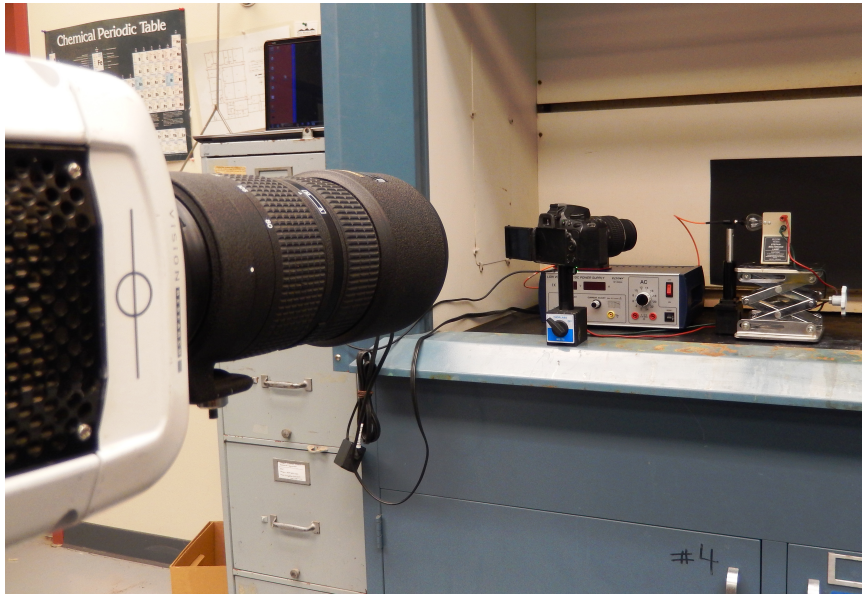
Figure 5.1: Experimental set-up for blackbody calibration.
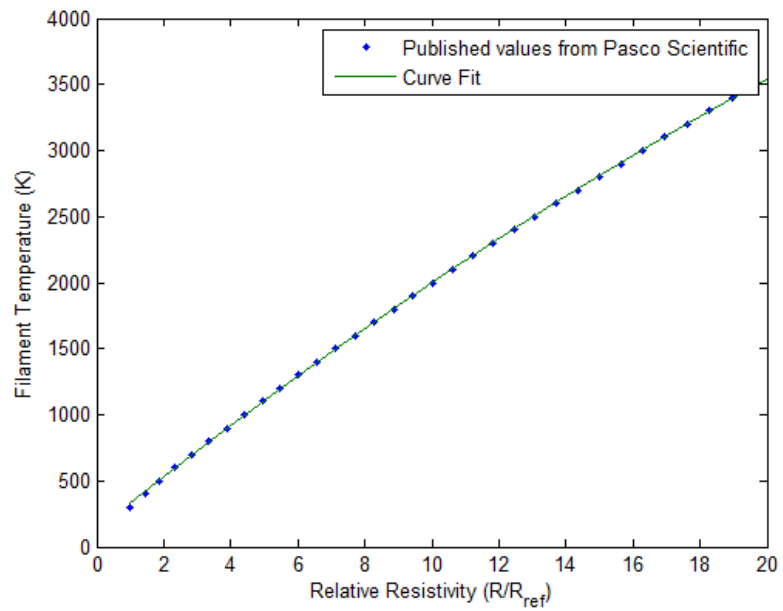
Figure 5.2: Filament temperature versus relative resistance for the TD-8555–data published by Pasco Scientific.

5.1.1 Blackbody Calibration of the Spectrometer

When collecting calibration spectra, ten samples of the spectrum were captured with an integration time of 17 ms. This integration time was selected so that the maximum calibration bulb intensity occurs just below saturation of the spectrometer, ensuring that the dynamic range of the spectrometer is most effectively utilized throughout all six levels. This is shown in Figure 5.3 with the peak of the maximum temperature's spectrum just below 1 (the value at which saturation occurs.) This method follows the procedure used by Densmore et. al, in which they selected specific bandpass filters for their two-color camera pyrometry system. The two filters were centered at 700 and 900 nm with pass-bands of 10 nm each [30]. The cameras used in this system were monochrome, meaning that the photo-sensors were not covered with the Bayer filter pattern. The responsivity of the photo-sensors (without a color filter array) extends outside of the visible region as far as 1100 nm. Densmore et. al then used different external filters to perform pyrometry with this system. The resulting calibration data for extension of this approach to the spectrometer is shown in Figure 5.4.
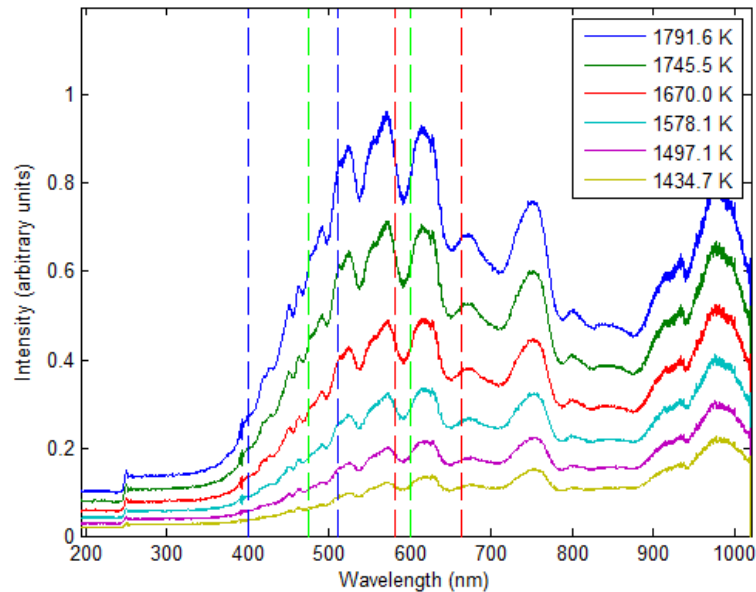
Figure 5.3: Tungsten bulb calibration spectra at various filament temperatures. Wavelength bands from FWHM of Phantom sensitivity shown with dotted lines.
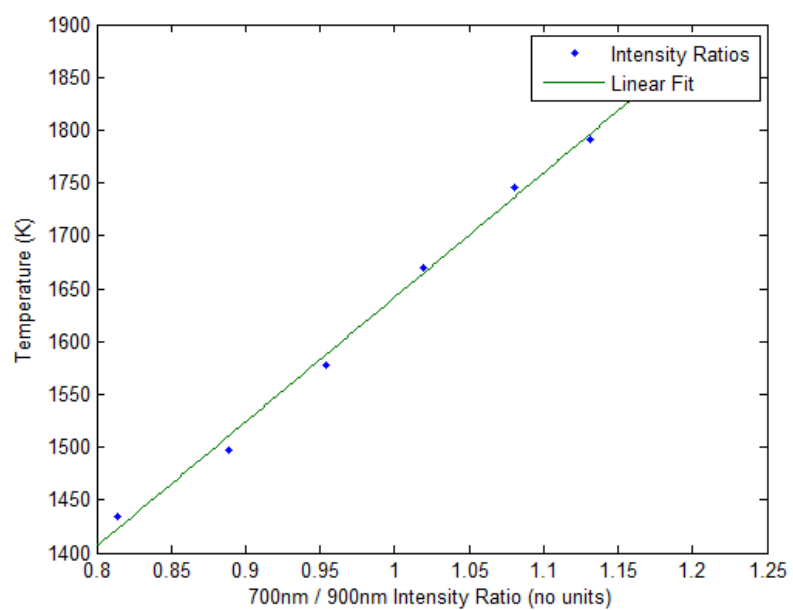
Figure 5.4: Tungsten bulb calibration curve from 700-to-900-nm intensity ratios.

5.1.2 Blackbody Calibration of the Phantom v611

Due to availability of the Phantom cameras, only one of the cameras was fully calibrated. Primary tests were performed with the calibrated camera, and the same techniques were applied to the other cameras in the later tests. To ensure repeatable settings in all data, including calibration and measurement images, all high-speed videos were saved with 0% brightness, gain, gamma, and saturation values of 1, 0 degrees of hue, and default (valued at 1 for red and blue) white balance values. These settings were found to affect the individual frames upon decomposition of the high-speed video and, therefore, are of importance in this process. Figure 5.5 shows the region in the tungsten filament high-speed frames evaluated during blackbody calibration.

Figure 5.5: *Left:* Cropped region evaluated in the blackbody (tungsten filament) calibration high-speed frames. *Right:* The color image of the tungsten filament during calibration.

The specific crop region shown in Figure 5.5 was selected to provide average red, green, and blue intensities in each frame at the different filament temperatures. Care was taken to ensure that only the most intense region of the filament was evaluated, as the edges would introduce directional radiation errors. Approximately 160 frames were evaluated at each filament temperature and the intensities were monitored for any brief anomalies in the sensor readings. Figure 5.6 shows the average red/green, blue/green, and blue/red ratios measured in the cropped region at each filament temperature. A highly linear relationship is present between filament temperature and each of the ratios.

These measured average ratios were then inserted on the left side of the following equation, which was developed by Densmore et. al [30] and is discussed in more detail in Section 5.5. As shown in Figure 5.7, the ratio of the integrals on the right side of the equation are known at the various theoretical tungsten filament temperatures.

$$\frac{Red}{Green} = \frac{\psi_r \int L(\lambda, T) x_r(\lambda) \, \mathrm{d}\lambda}{\psi_g \int L(\lambda, T) x_g(\lambda) \, \mathrm{d}\lambda} \tag{5.1}$$

29
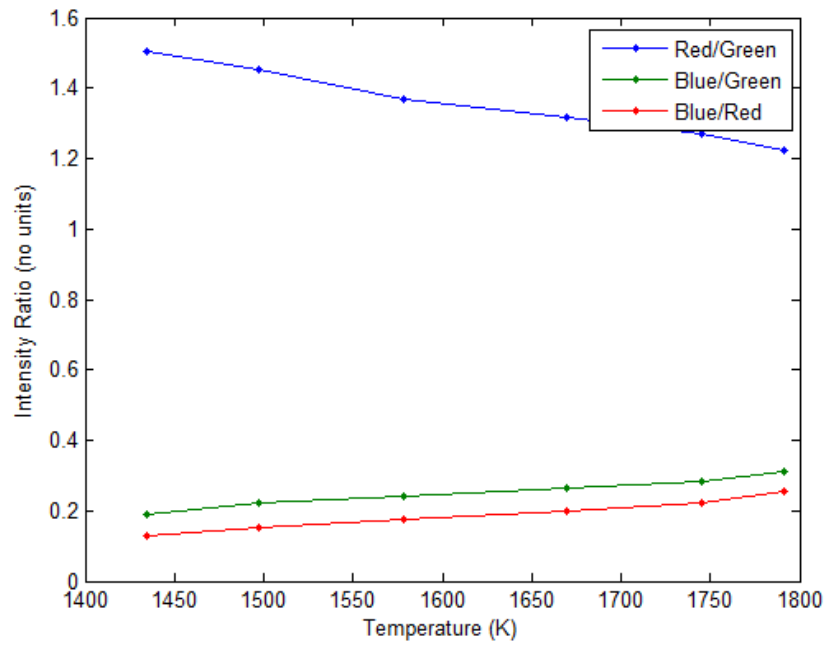
Figure 5.6: Intensity ratios from the Phantom v611 without ambient lighting.
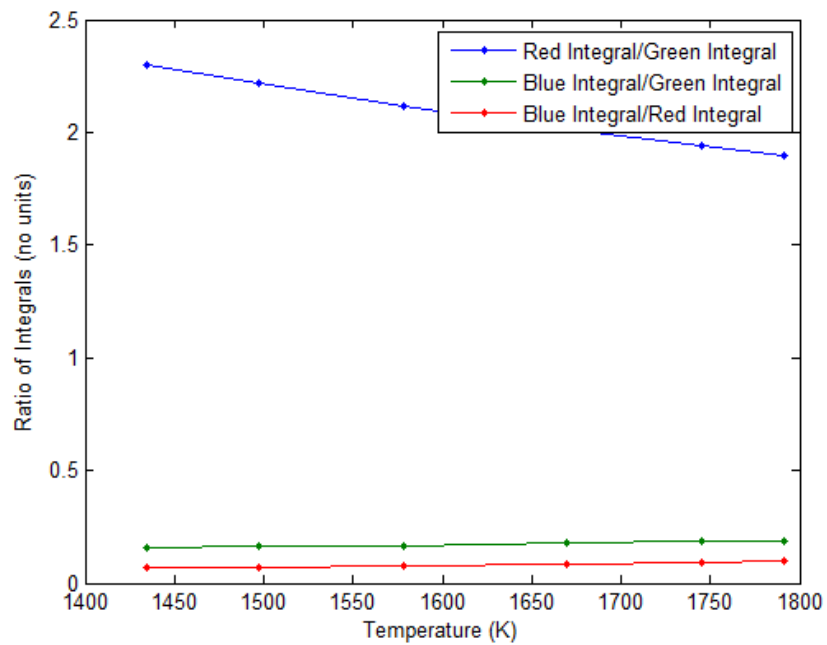
Figure 5.7: The calculated ratios of the integrals shown in Equation 5.4.

Knowing the color ratios on the left side and the ratio of the integrals on the right side as functions of temperature, the calibration factors $\frac{\psi_{red}}{\psi_{green}}$, $\frac{\psi_{blue}}{\psi_{green}}$, and $\frac{\psi_{blue}}{\psi_{red}}$ can also be calculated as functions of temperature as shown in Figure 5.8.
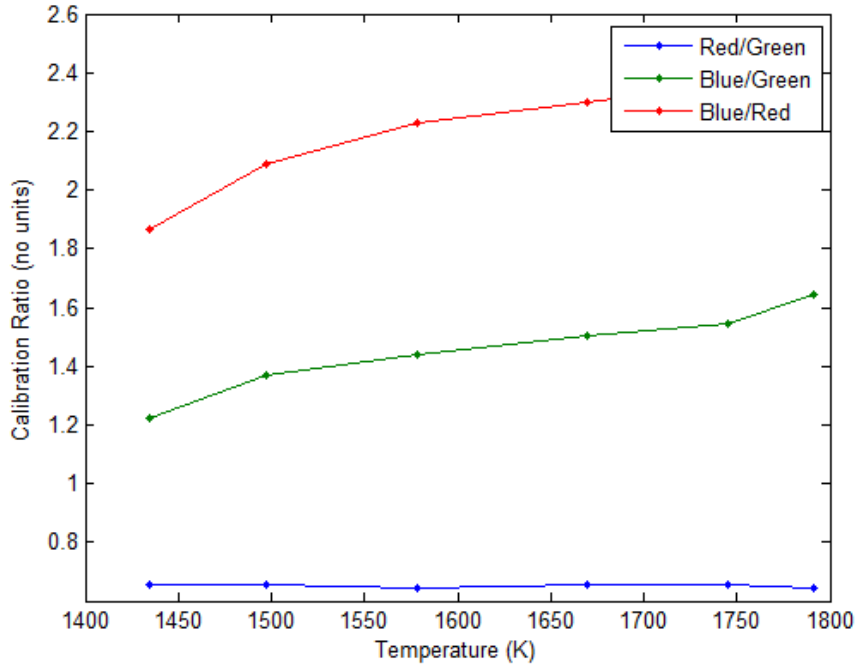
Figure 5.8: The calculated calibration factor ratios.

These calibration factors were then used to solve for the entire right side of the equation as a function of temperature, which is shown in Figure 5.9. The linear fits applied to the three sets of ratios were then used in future tests to measure temperature based off of the observed color ratios. The calibration program shown in Appendix B performs the calibration calculations to automatically produce calibration curves when tungsten data is provided. It is seen from Figure 5.9 that a larger variation in intensity ratios exists at lower temperatures and narrowing occurs at the higher temperatures. In comparison with Figure 5.10, the same trend exists between the Phantom calibration fit and the theoretical ratios for a blackbody. While the exponential shape is not common to both plots, the order of intensities (red/green, blue/green, and blue/red, from largest to smallest) does match.
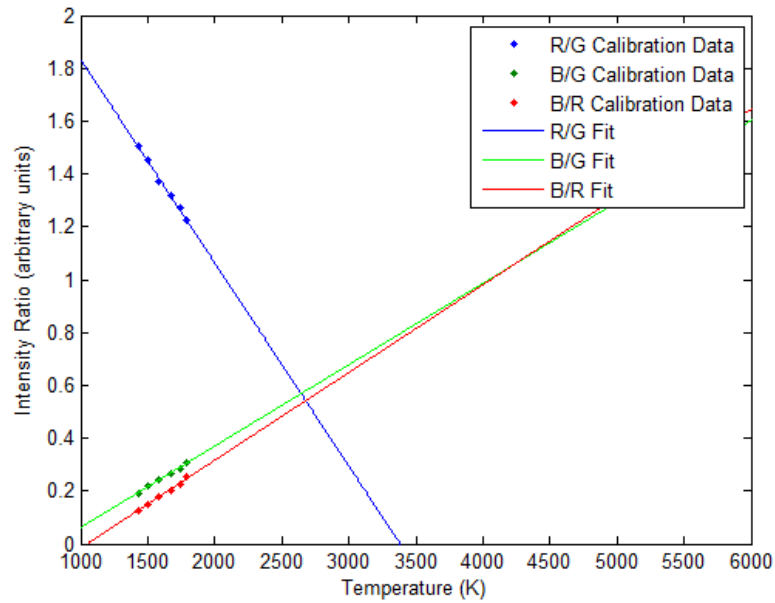
Figure 5.9: The full calibration fit for the Phantom v611, calculated from the right side of Equation 5.4. The linear fit seen here is used in future tests to measure temperature.
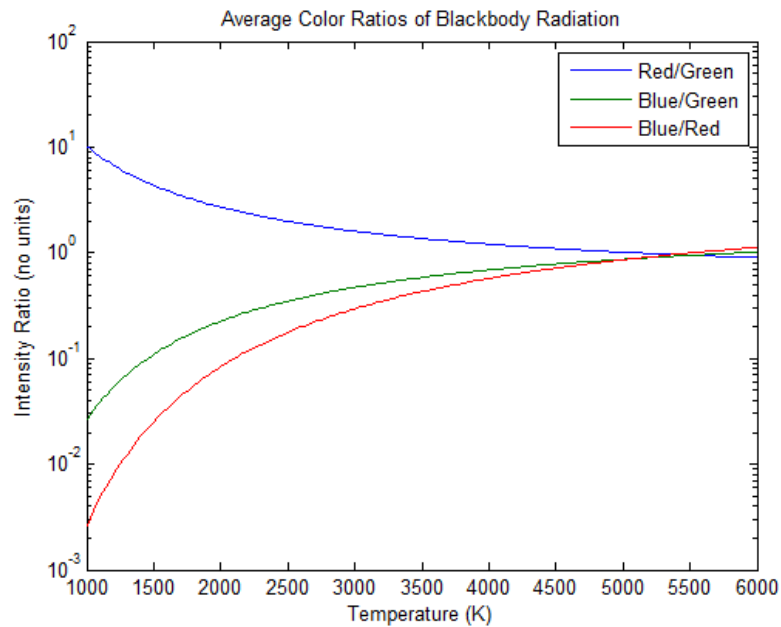
Figure 5.10: Red-to-green, blue-to-green, and blue-to-red color ratios for a blackbody as a function of temperature as calculated from Planck's Law. Note that the ratios in this plot and the calibration plot follow the same trend.

5.1.3 The Effects of Ambient Lighting and the Cosine Corrector

The effects of ambient lighting and use of a cosine corrector were also studied using the tungsten bulb. Since the foundational aspect of this temperature measurement technique is to measure filtered light output, ambient lighting has the potential to cause large errors. In addition, Thorlabs manufacturers a cosine corrector to be used on free-space spectral measurements, such as those seen in an explosion. To determine the necessity of using a cosine corrector in future explosives testing, its effect on the tungsten bulb spectra was also inspected. Figures 5.11-5.13 show the effects of both ambient lighting and cosine corrector use on the tungsten bulb's spectra. Fluctuations are noticeable at lower temperatures, but are negligible at the higher temperatures. Since this temperature measurement technique is meant to be used for explosions and rocket exhaust, with temperatures ranging from 2000-6000K, this lower-temperature variation can be ignored.
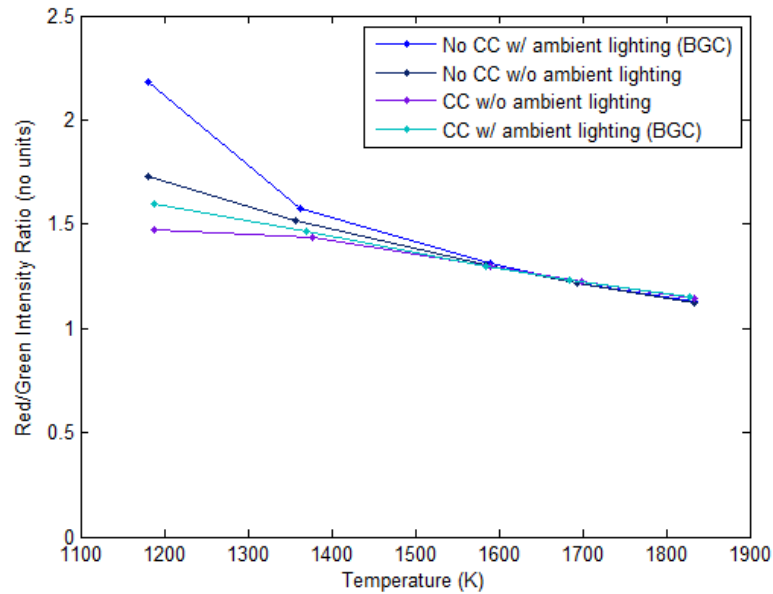
Figure 5.11: Ambient lighting and cosine corrector effects on red/green spectral intensity ratios.
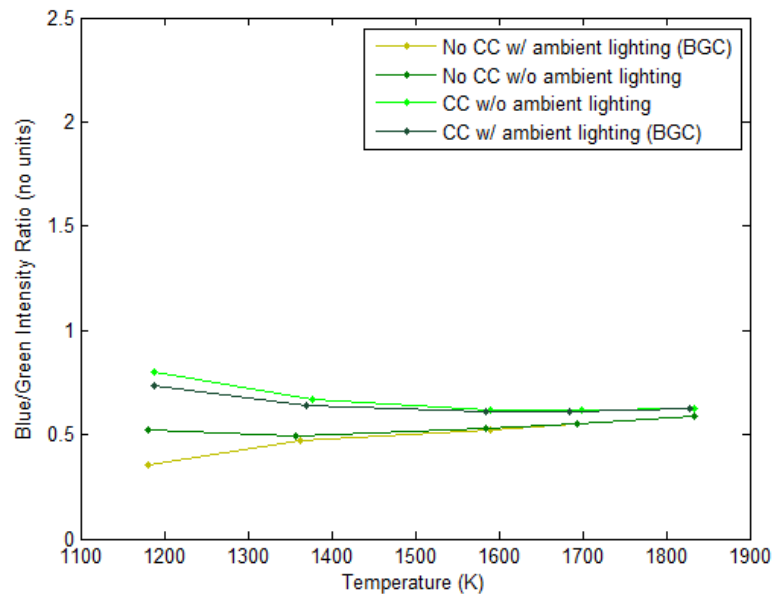
Figure 5.12: Ambient lighting and cosine corrector effects on blue/green spectral intensity ratios.
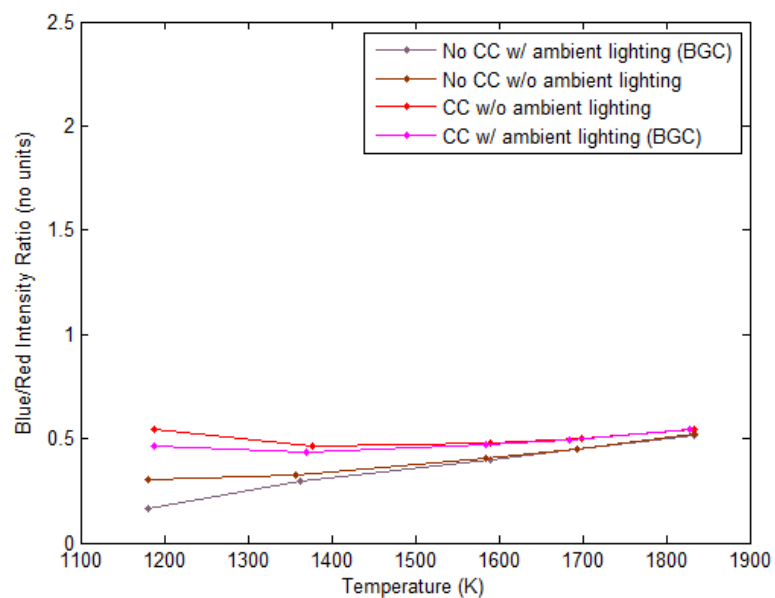
Figure 5.13: Ambient lighting and cosine corrector effects on blue/red spectral intensity ratios.

Figure 5.14 shows the effect of ambient lighting on Phantom camera intensity data. Negligible variation is seen from the presence of ambient lighting in the blue/green and blue/red intensity ratios. However, the red/green intensity ratios vary greatly due to the presence of ambient lighting. In conclusion, it is generalized from this comparison that, at the extreme temperatures of explosives and rocket exhaust, ambient lighting can have an effect on temperature determination. It is hoped that the negligible effect on the blue/green and blue/red ratios will counteract the variation seen in the red/green ratios. As a precaution, however, energetic material testing was performed with minimal ambient lighting whenever possible.
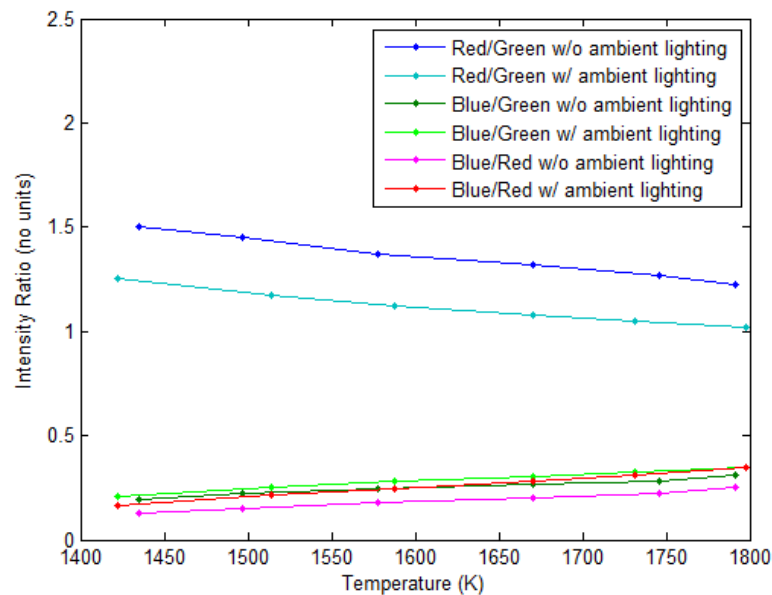
Figure 5.14: Ambient lighting effect on Phantom intensity ratios.

5.2   Decomposing RAW Cine Files into RAW Images for Processing

Phantom high-speed cameras output video in the form of cine files. These cine files, similar to other video file extensions, are a collection of frames from the camera displayed in sequenced video. For this research, all high-speed videos were captured using the raw cine format. This format stores the frames as raw data, a smaller file size than the demosaicked format, and performs the corrections and demosaicking upon viewing or conversion in the Phantom software. Since the raw pixel data was desired to perform temperature calculations, this raw cine format was the best option available.

In order to process the cine file for temperature, it first needed to be decomposed into its respective frames. This was performed by modifying MATLAB software development kit (SDK) example code entitled "Read Cine File Image" published by Vision Research. This object-oriented code references libraries of functions published by Vision Research to perform specific tasks. The example code was converted into a for loop that reads the cine image, performs no demosaicking, and outputs the image to a TIFF file for all frames in the video. Only one major change was made to the example code to perform the necessary functions–when reading the cine image into the buffer, the code is set to perform "no demosaicking" (PhFileConst.GCI INTALGO is 6.) An output was also added for the value of PhFileConst.GCI CFA so that the filter pattern could be confirmed to ensure correct processing methods. For the videos from the Phantom v611, the CFA filter pattern was found to be the Bayer filter pattern, as expected. The pattern starts with the top left pixel being green, and the first row alternating green and blue, as shown in Figure 5.15.
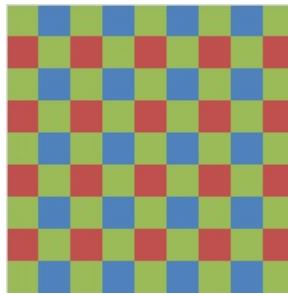
Figure 5.15: A portion of the Bayer filter pattern used in the Phantom v611. The top left pixel is green and the first row alternates between green and blue.

5.3 Separating Pixels According to the Bayer Filter Pattern and Calculating Temperatures

Upon decomposition of the cine video into TIFF images, the images then needed to be separated into 3x3 matrices for temperature calculations. The analysis region was chosen to be 3x3 matrices based on the work of Densmore et. al [22]. Figure 5.16 shows the four types of 3x3 matrices that exist in the Bayer filter pattern shown earlier. The indices of the top left pixel's (TLP's) row and column are always odd or even, as displayed in the table.

Type	Row index of TLP	Column index of TLP
1	odd	odd
2	odd	even
3	even	odd
4	even	even

Figure 5.16: The four types of 3x3 matrices that exist in the Bayer filter pattern. The indices of the top left pixel are tabulated based on being odd or even.

Using this knowledge, a for loop was utilized to convert the original high-speed frame into a new temperature image–the full code is located in Appendix C:

1. Define the row and column indices of the top left pixel of the first 3x3 matrix (1,1)

2. Determine the type of 3x3 matrix based on the row and column indices being odd or even

3. Depending on the type of 3x3 matrix, calculate the average red, green, and blue intensities

4. Calculate the color ratios from these intensities

5. Use the three color ratios to calculate three temperatures

6. Average the three temperatures calculated for the 3x3 matrix

7. Create a new image where the center cell of the 3x3 matrix is filled with the same average temperature

8. Cycle through the first row of 3x3 matrices by incrementing the column index of the matrix by 1 and repeating the previous steps

9. Cycle through the rest of the rows by incrementing the row index by 1 and returning to the column index of 1 at the end of each row

10. At the end of each frame analysis, display the temperature matrix created in step 7 using a color map and capture it for a video frame

11. At the end of the last frame, create a video of the frames captured in the previous step

An additional capability was added to the code that uses cropping to perform a temperature history analysis. In addition to creating a temperature video from the high-speed frames, the user crops the first image in the area of concern (i.e. the inner circle of the primer face) and the program crops all other images in the same location. The same process enumerated earlier is performed for this cropped section and the average temperature in the entire cropped region is recorded with respect to time based on the video frame rate. The temperature history allows for an overall trend of the temperature in the specified region to be observed, which can aid in detection of processing errors and anomalies.

5.4 Temperature Measurement from Spectra

The spectra radiated from an event have often been used as temperature indicators when conventional temperature measurement techniques are insufficient. Like the three-color method discussed in Section 5.5, spectra temperature measurement techniques do not require contact with the subject material, thereby reducing replacement/maintenance costs and time. Two spectra techniques are presented and used as comparions for the three-color technique: the two-color ratio technique and the visible spectrum blackbody fitting (VSBF) technique.

5.4.1 Two-Color Ratio

The two-color ratio technique relates the ratio of two narrow wavelength bands to the temperature of the calibration blackbody. Densmore et. al used this method to measure the fireball temperatures of 815-g TNT charges [30]. They used interchangeable filters at 700 and 900 nm with 10-nm FWHM to restrict the incoming light into the high-speed cameras.

In this research, this technique was extended to the spectra measured during an event. The spectra in the 700±5 nm and 900±5 nm bands were used to measure the color ratio. Prior to measurement, as with all other techniques, calibration was performed by viewing the tungsten filament bulb. The tungsten filament spectra were then corrected with respect to the spectrometer's responsivity, shown in Figure 3.1, by dividing the actual measured spectrum by the responsivity. The measured color ratio was related to the theoretical filament temperature, and a linear fit was applied to the data. Using the linear fit, future measured color ratios (calculated after subtraction of the background spectrum

and correction with respect to the spectrometer's responsivity) were converted into temperature.

5.4.2 Visible Spectrum Blackbody Fitting

The visible spectrum blackbody fitting (VSBF) method calibrates a measured spectrum and fits the data to a blackbody curve. By comparing the fitted equation to Planck's Law, the temperature can be calculated. This method was used by Lebel et.al to study the fireball temperatures of 175-g Detasheet-C charges. In order to more closely match the measurements made by the visible-radiation-viewing cameras, the spectra were evaluated only in the range of 500-950 nm as discussed by Lebel et. al [3].

Prior to calculating temperature from the measured spectra, the system was calibrated with the Pasco Scientific tungsten filament lamp discussed in Section 5.1 to determine the spectral sensitivity of the spectrometer. The spectrally-resolved spectrometer sensitivity was calculated as the ratio of the theoretical blackbody spectral radiance $B(\lambda)$ to the actual spectra collected from the tungsten lamp $I_s(\lambda)$ as shown in Equation 5.2. An example of this sensitivity calculation is shown in Figure 5.17.

$$S(\lambda) = \frac{B(\lambda)}{I_s(\lambda)} \tag{5.2}$$

This sensitivity as a function of wavelength was then multiplied by the measured spectrum (i.e. shotgun shell primer spectrum) after subtracting the background spectrum from it. The calibrated test spectrum was fitted to a version of Planck's Law with modified constants, as shown in Equation 5.3 [3], using the non-linear regression fit MATLAB function. An example of a primer spectrum calibrated using the sensitivity and fitted to Planck's Law is shown in Figure 5.18.

$$B(\lambda) = \frac{C_a}{\lambda^5 (e^{C_b/\lambda} - 1)} \tag{5.3}$$

From Planck's Law, shown in Section 5.5, the fitted coefficient C_b is equal to $\frac{C_2}{T}$. Knowing the fitted coefficient C_b and the theoretical coefficient C_2, the temperature can be directly calculated.
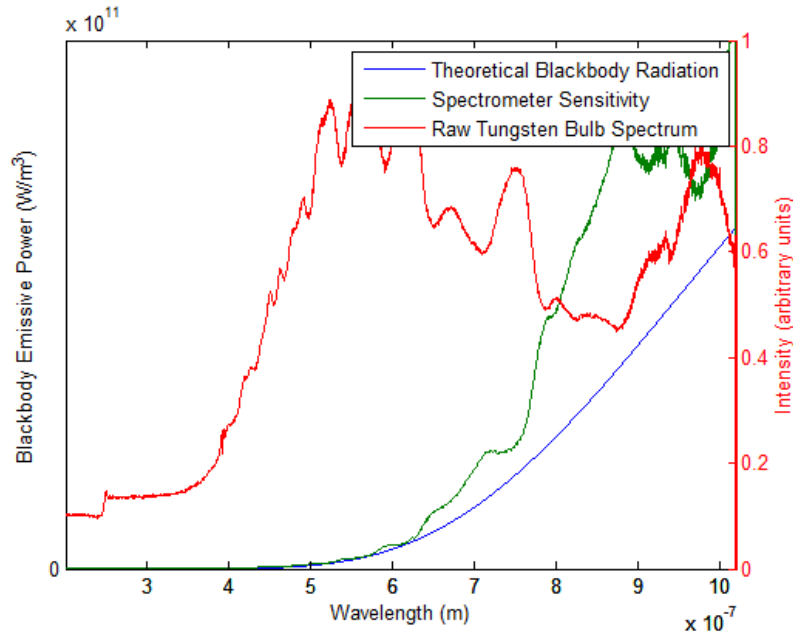
Figure 5.17: A plot of the raw tungsten bulb spectrum at a known temperature, the theoretical radiation of a blackbody at the same temperature, and the ratio of the two as calculated using Equation 5.2.
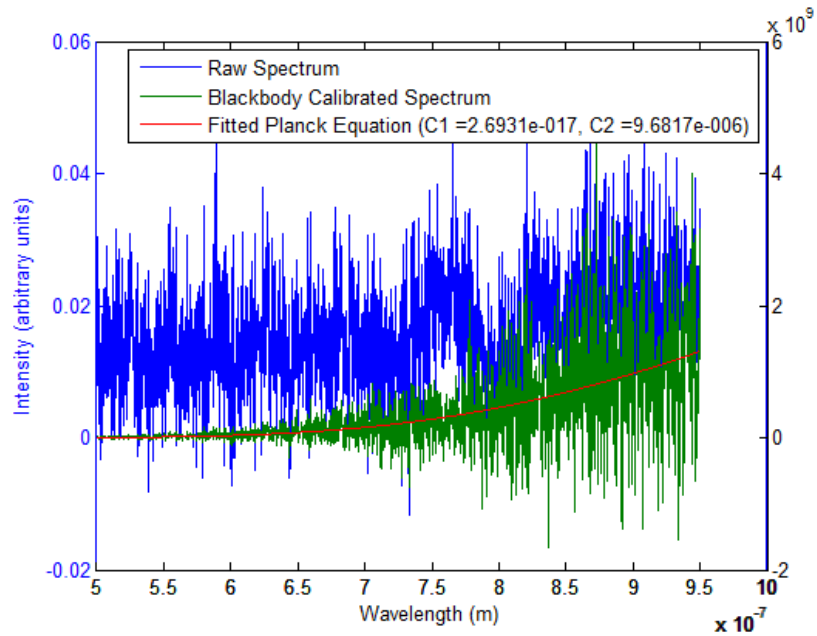
Figure 5.18: A plot of a raw primer spectrum, the calibrated spectrum, and the fit to Planck's Law. The values for the two fit constants for this particular spectrum are shown in the legend.

5.5 Temperature Determination from RAW Images

Upon decomposition of RAW cine files into frames in the form of TIFF images, temperature calculations were then performed according to Densmore et. al. In the calibration equation used for this technique, Densmore combined the spectral sensitivity of the camera sensor (available from the manufacturer for Phantom cameras–an example of which can be found in Figure 3.4) with Planck's law in a relationship that can be used to calculate the overall calibration factor of a two–or more–color pyrometry system. The overall calibration factor takes into account the unknown light intensity variations, lens optics, and internal electronic factors of the camera. The equation published by Densmore et. al [30] is as follows:

$$\frac{Red}{Green} = \frac{\psi_r \int L(\lambda, T) x_r(\lambda) \, \mathrm{d}\lambda}{\psi_g \int L(\lambda, T) x_g(\lambda) \, \mathrm{d}\lambda} \tag{5.4}$$

where the red-to-green ratio is determined from the green and red channels of a blackbody image/video, $L(\lambda, T)$ is the spectral radiation from Planck's Law,

$$E_{b\lambda}(\lambda, T) = \frac{C_1}{\lambda^5 \left(e^{\frac{C_2}{\lambda T}} - 1 \right)} \tag{5.5}$$

where

$$C_1 = 3.74177 \times 10^{-16} W \cdot m^2 \qquad C_2 = 1.43878 \times 10^{-2} m \cdot K$$

x_r and x_g are the spectral sensitivities of the camera, and

$$C_{rg} = \frac{\psi_r}{\psi_g} \tag{5.6}$$

is the unknown calibration factor to be calculated. When a blackbody at known temperatures is imaged, the measured color ratios and known temperatures (such as those shown in Figure 5.6) can be used in Equation 5.4, evaluated over the visible spectrum, and solved for C_{rg}. Upon determining the calibration factor as function of temperature, the temperature of an approximated blackbody can be determined by referencing the temperature that corresponds to the measured color ratio.

CHAPTER 6

EXTENSION TO A HIGH SPEED COLOR VIDEO CAMERA

The energetic materials studied included shotgun shell primers, pyrotechncis, and NONEL shock tube. Due to the minute durations of these events, it was necessary to use a high-speed camera in order to temporally resolve the events fast enough for processing. It is important to note that this did not affect the temperature calculation process in any way other than altering the camera-specific spectral sensitivity and blackbody calibration data.

6.1   Shotgun Shell Primers

The first set of temperature measurement testing was performed on Remington 209 Premier STS shotgun shell primers. According to the MSDS, the energetic materials present in these primers are lead styphnate (0.2-0.8% by complete primer weight), lead trinitroresorcinate (no weight data published), and tetrazene (less than 0.1% by weight.) The primers were held in a fixed position using a firing gun (similar to a flare launcher) directed at the Phantom camera, as shown in Figure 6.1.

The spectrometer fiber end was positioned a few centimeters away from the primer face to collect spectra during the event, as shown in Figure 6.2. The angle between the primer centerline to the camera and the primer centerline to the fiber was minimized to ensure minimum geometry error in the data. An example of the spectra from this set of testing can be found in Section 4.2.2.

The following four sequential frames show the original high-speed video frame (*left*) and calculated temperatures (*right*) in frames 1, 2, 13 and 20, respectively, from a primer test. The primer fireball progresses as expected–it begins at a temperature much higher than the surrounding temperatures, expands, and begins to cool. The surrounding ambient temperatures are not correctly calculated because the technique used is only suited for measuring extreme temperatures. Ambient temperatures, such as those in the surrounding lab air, are not high enough to begin radiating in the visible region. Note that, in Figure 6.3, high temperatures are shown in white, cool temperatures are in black, and the other
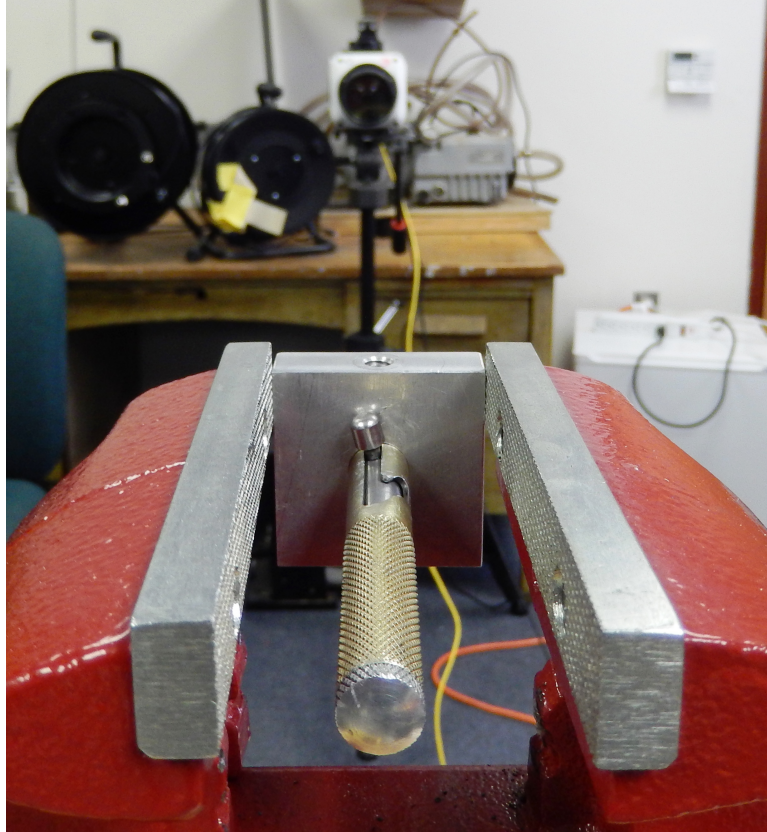
Figure 6.1: The firing gun aimed at the Phantom camera, positioned approximately 2 meters away.
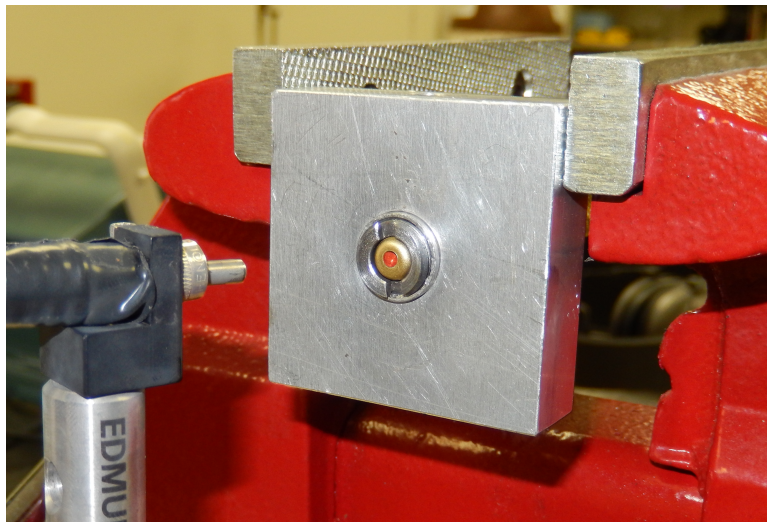
Figure 6.2: Primer loaded in firing gun just before a shot. Note the spectrometer fiber end directed at the primer.

temperatures vary from red to yellow. The object in the bottom left of each image is the optical stand that held the fiber optic in place during the event. It is important to note that the images are extremely dark because the video was taken with extremely low light inlet. Low light inlet is important for optimizing the camera sensor's response without saturating the pixels. Even though it is difficult to discern the primer from the surroundings in the first two frames shown, the camera is able to process these frames as effectively as the other frames.

According to a report by the Australian Department of Defence, the fireball temperature of a similar primer was studied using a radiant energy technique similar to the three-color technique. The energetic material studied, called an M42 primer, is designed to produce a large amount of gas, and is generally comprised of barium nitrate (22.0% by weight), antimony sulphide (10.0%), lead styphnate (53.0%), tetracene (5.0%), and aluminum (10.0%) [31]. Although this primer does not possess the same exact composition as the Remington primers, it serves as an order of magnitude value with which a comparison can be made. According to Kelly, this M42 primer produces gases of 2650 °C (2923 K) [32]. When compared with this value, the three-temperature technique measured an initial peak temperature of 2059 K and an average event temperature of 1850 K–only 29.6% and 37% lower, respectively, than that measured by Kelly. There are two main factors that likely contributed to this difference:

1. While Kelly utilized a similar radiant energy temperature measurement technique, he measured only one color ratio (as opposed to three) using two photomultipliers–one at 230 nm (UV) and the other at 1200 nm (IR.)

2. The M42 primer used by Kelly did not possess the same composition as the Remington primers and therefore cannot provide a direct comparison. It serves merely as an order-of-magnitude check.

In addition to processing the high-speed primer data to show spatial resolution of temperatures, the cropping-method MATLAB code discussed in Appendix C was used to measure the average temperature of the fireball region in each image. Since each image is another step in time equal to the inverse of the frame rate, this process produced a temperature history of the fireball and an overall average temperature of the entire event. In cropping the images, only the region within the primer's outer circular shell (shown in Figure 6.4) was evaluated to avoid including the fiber stand and other unrelated items in the scene. This region in each image was then processed into a temperature matrix of which the average temperature was recorded. Figure 6.6 shows the average temperature in each image as a function of time from the beginning of the event. The temperatures listed with the test number are the average temperatures throughout each entire shot. These temperatures are also the values to which the temperatures
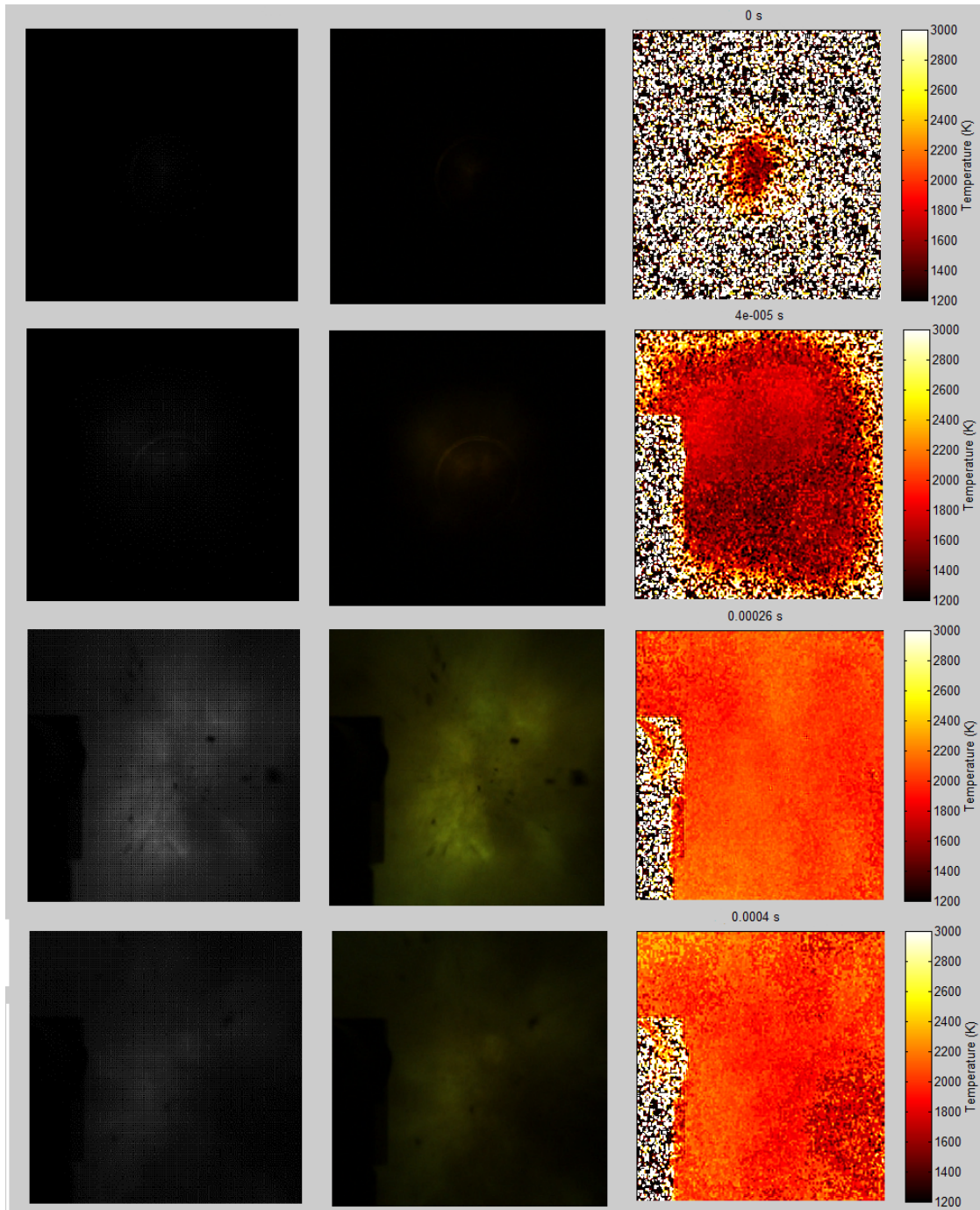
Figure 6.3: Four frames from a high-speed temperature video taken during a primer shot. The first column shows the raw frames (no demosaicking), the second column shows the color video, and the third column shows the calculated temperature images. *First image:* Initiation of the primer. *Second image:* Expanding fireball with hottest temperatures at the core. *Third image:* Maximum event temperatures reached in fireball. *Bottom right:* Expanding gases cooling at the outer edges.

calculated using the two-color spectrometer technique will be compared, due to lack of spatial resolution in the spectra.
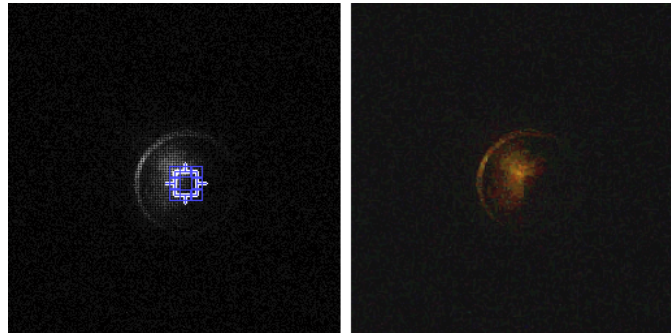
Figure 6.4: *Left:* An example of the crop region used to calculate primer temperatures using the three-color method. Right: The same image in color, with brightness, saturation, and gain settings adjusted for easier viewing.

From Figure 6.6, it is seen that the temperature trends observed with the three-color pyrometry technique are highly repeatable. An initial peak of about 1500-2500 K occurs, after which a much slower heating occurs with its peak at about 2150 K. The differences between the initial peak temperatures are attributed to the variable qualities of the primer. The average initial peak temperature is estimated at 2250 K–a 23% difference when compared with the value published by Kelly.

Spectra was simultaneously collected during this primer testing using the spectrometer described in Chapter 3. The smaller core diameter fiber was positioned with its end aimed at the center of the unfired primer approximately 2 cm away, slightly offset so as not to block the view of the head-on-viewing Phantom. Various integration times ranging from 100 ms to 10 s were used to observe the corresponding changes in the data. The spectrometer data was collected for comparison the temperatures measured with the Phantom. The two techniques discussed earlier (VSBF and two-color ratio – both in Section 5.4.1) were performed on the spectra.

Figure 6.6 shows the temperatures calculated with the three-color, black-body fitting, and two-color methods. Unfortunately, due to the much slower integration time of the spectrometer (equivalent to a long exposure in a camera), the temporal resolution of the measurements was not as satisfactory as the high-speed camera measurements. Because of this, the spectra measurements show an average of the temperatures over the integration time steps.

It is apparent that the quick exposure time of the high-speed camera resolves interesting waveform characteristics that the spectrometer cannot resolve. Ignoring this, however, all three data sets agree relatively well. The two-color and
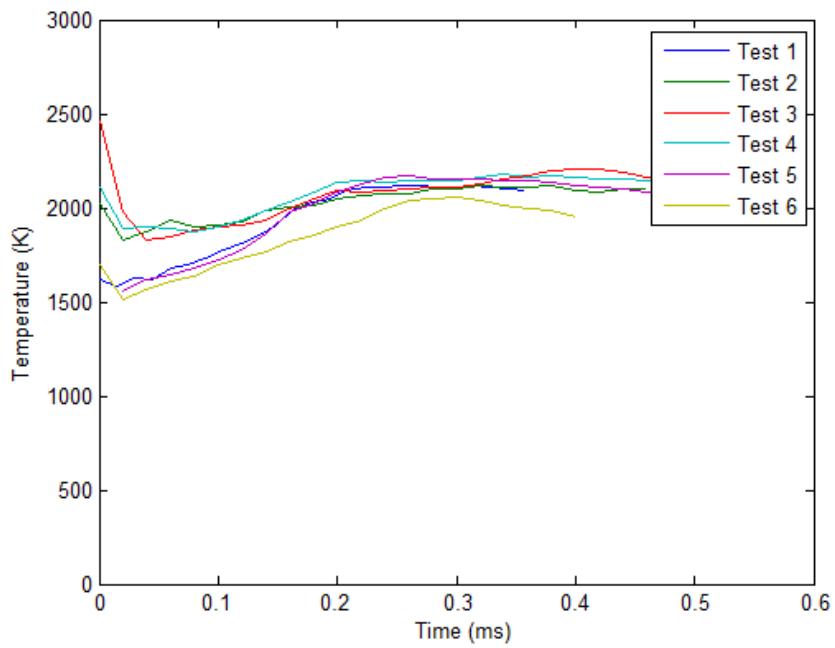
Figure 6.5: Primer temperature history obtained by calculating average temperature in the fireball region for each high-speed frame.
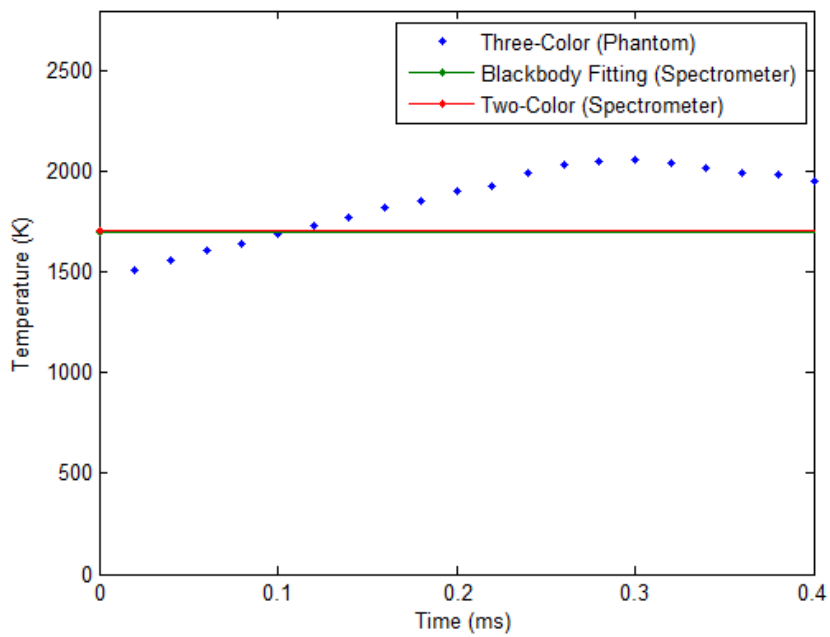
Figure 6.6: Primer temperature history calculated using all three methods.

blackbody fitting methods measure nearly the same temperature, which does, in fact, agree well with the average three-color temperature. Unfortunately, the data shown for the spectra methods consist of only a few data points (only one of which is shown on this plot due to the time scale)–hence, these measurements are shown with a straight line. The average three-color temperature is only about 150 K more than the spectrometer measured temperatures.

6.2   Pyrotechnic Mixture

The shotgun shell primer events were observed to be extremely short duration events, making it difficult to reliably compare temperatures measured from various methods. While the high-speed camera was able to temporally resolve the event quite easily, the spectrometer did not receive enough incoming light to produce similarly-time-resolved data.

In an effort to test the three-color technique more effectively, a slower-burning reaction was chosen. A common pyrotechnic mixture of potassium chlorate ($KClO_3$) and sucrose (table sugar–$C_{12}H_{22}O_{11}$) was prepared at oxygen balance so that the heat output would be optimal. Because of the slower propagation rate of this mixture, it is defined as a deflagrating low explosive. Figure 6.7 shows the prepared mixture ready just prior to igniting the fuse.
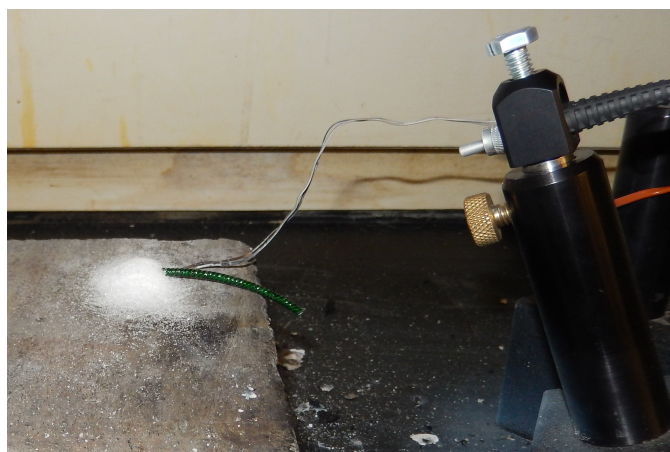
Figure 6.7: Potassium chlorate and sucrose mixture ready for a shot. Note the buried bare-metal thermocouple and the green fuse used for initiation.

Figure 6.8 shows the crop region used to calculate the three-color temperatures. Figure 6.9 shows the temperatures calculated from each of the three methods. The three-color method and blackbody fitting method agree well with

each other, while the two-color method consistenly measures approximately 700 K lower than the blackbody fitting method. While the blackbody fitting method occasionally produces unrealistic values due to the fitting aspect, it appears to be the more accurate method. The increase in variation between the three-color method and blackbody fitting method is attributed to the test setup. The pyrotechnic mixture was initiated in a line perpendicular to the camera's line of sight. The spectrometer fiber was aimed at the right end of the pyrotechnic mixture initiation path. Therefore, as the reaction progressed, it occurred progressively farther away from the spectrometer fiber. Due to the inverse square law of radiation, it would be expected that the radiation intensity would decrease and, therefore, result in lower temperature readings–this is the case as seen in Figure 6.9.
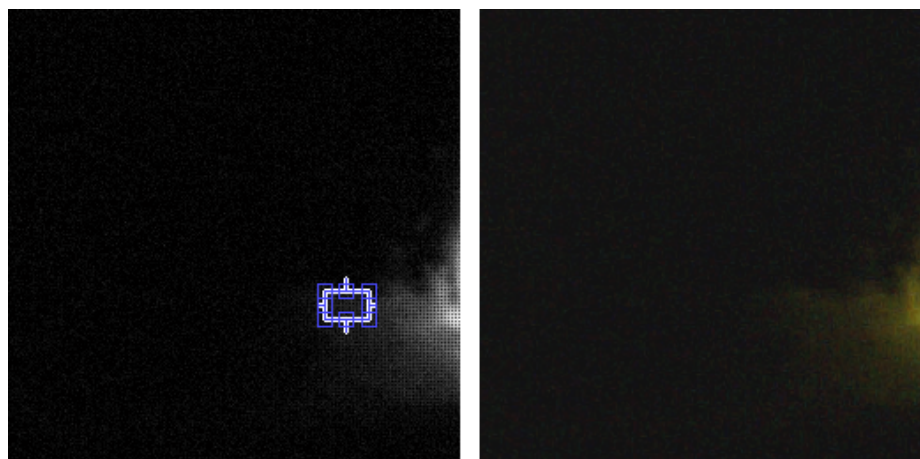
Figure 6.8: Crop region used to calculate the three-color temperatures during this particular pyrotechnic test.

The following four sequential frames show the original high-speed video frame (*left*) and calculated temperatures (*right*) in frames 1, 250, 1250 and 1800, respectively, from a pyrotechnic test. The pyrotechnic flamel progresses right to left and remains at the same average temperatures throughout the event. Again, the surrounding ambient temperatures are not correctly calculated as with all other measurements in this research.
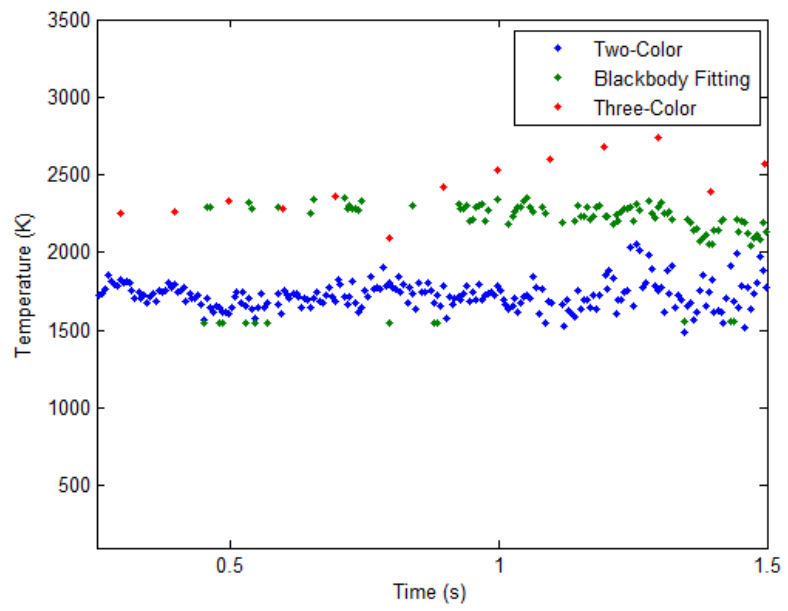
Figure 6.9: Temperature history comparison for one pyrotechnic test.
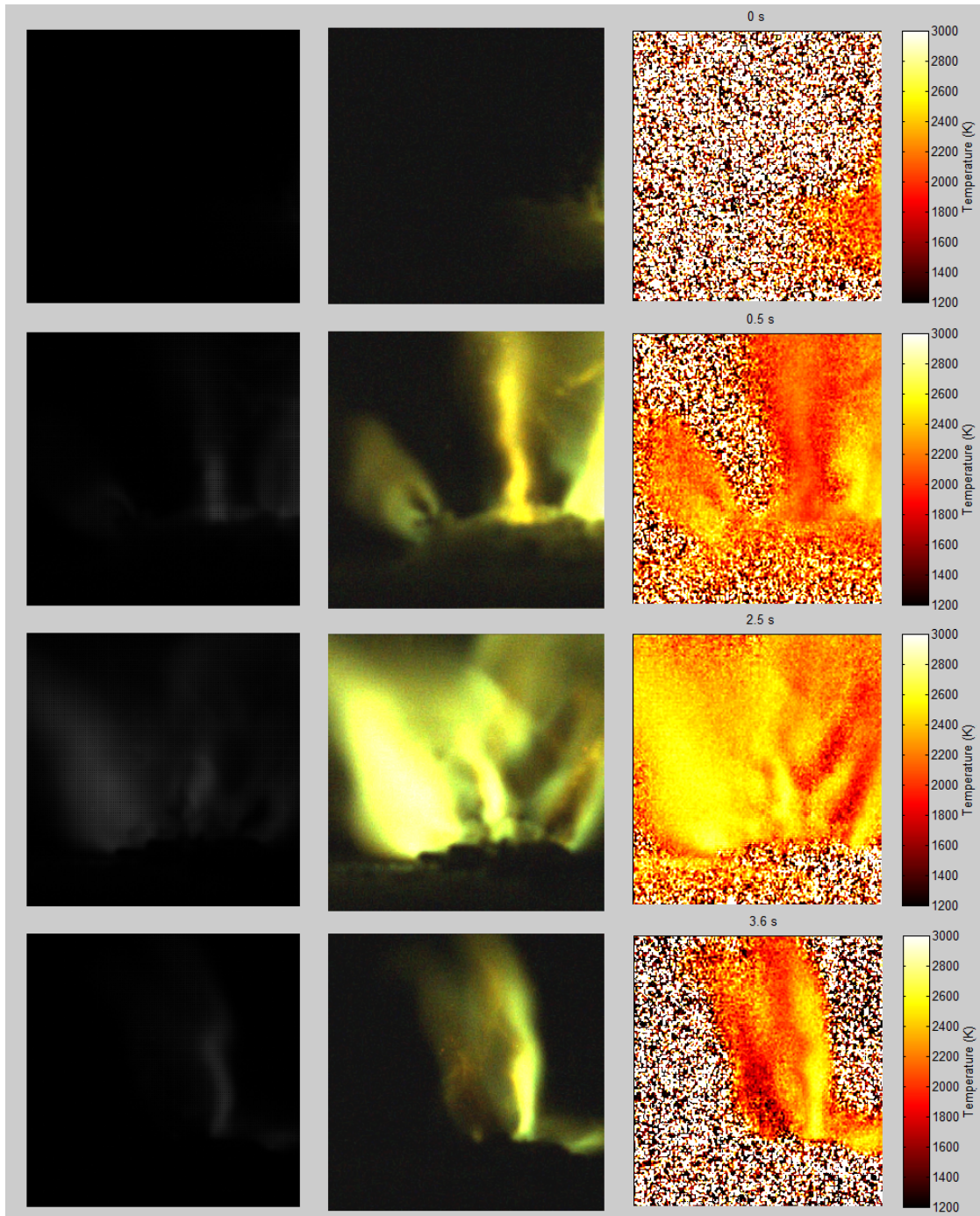
Figure 6.10: Four frames from a high-speed temperature video taken during a primer shot–the corresponding temperature images are shown on the right. *First image:* Initiation of the pyrotechnic. *Second to fourth images:* Examples of complex flame structures shown for comparison between the high-speed video and the calculated temperature video.

6.3 NONEL

To further explore the compatibility of this system with high explosives, temperature measurements were taken of NONEL. Discussed in greater detail in Section 4.2.4, this non-electric initiation system consists of a plastic tube coated on the inside with HMX and aluminum. The NONEL was secured in an optical stand directed toward the high-speed Phantom V7.1 camera approximately 3 meters away. At the smallest resolution (128x128), the highest frame rate possible was 66,666 fps. Due to the high-speed detonations of NONEL and the limited frame rate of the high-speed camera being used, the time duration of the detonation flash at the open end was visible in only one frame. In addition, the outer diameter of the NONEL is only about 1/8 inch; at 3 meters away, this is an extremely small target area even at maximum zoom on the camera. Therefore, the temperature measurements of the NONEL were not temporally-resolved and resulted in only a few spatially-resolved temperature measurements per shot.
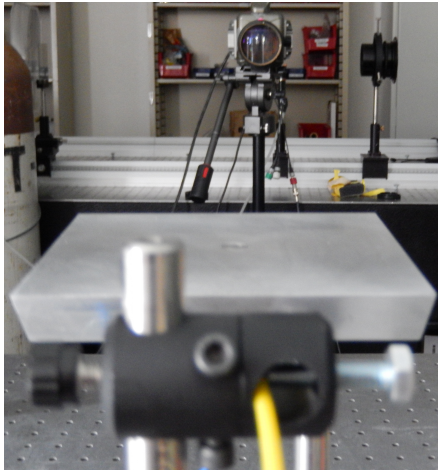
Figure 6.11: Test set-up showing NONEL tube (yellow) loaded into the optical stand. The aluminum plate in front of the NONEL did not obstruct the field of view of the camera–it was used for simultaneous data collection of a different characteristic of NONEL.

Figure 6.12 shows the raw and color images of the flash, while Figure 6.13 shows the calculated temperature image. The three-color method calculated an average peak temperature of 3595 K with a range of 121 K. Hegde et. al published a measured temperature of 5950.72 K, which was also measured using spectra and Planck's blackbody radiation law [33]. DaBin measured temperatures of 2000-2500 K using a modified sodium line reversal method and two-line spectroscopy method [34]. The three-color measured value of 3595 K agrees well with these two sources, as it easily fits within the range of published values.
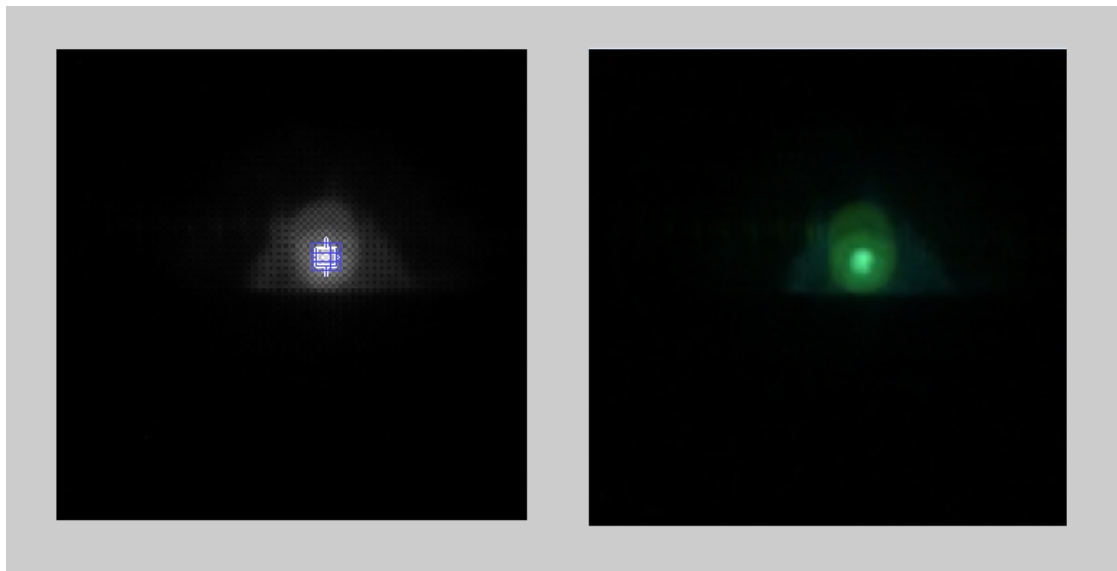
Figure 6.12: *Left:* Raw frame of detonation flash showing crop region at core of NONEL shock tube. *Right:* Same image in color with settings adjusted for better visibility.
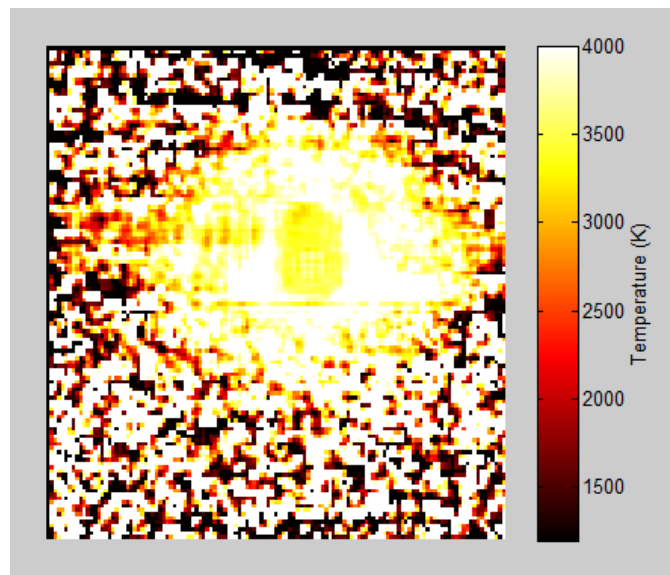
Figure 6.13: Calculated temperatures from the raw image. The average temperature in the cropped region is 3632 K. Note that the aluminum plate is visible in this image, as well as Figure 6.12.

CHAPTER 7

SOURCES OF ERROR AND AREAS FOR FUTURE IMPROVEMENT

The three-color method presented here that is based on the color filter array of a digital color camera has been shown to accurately measure high temperatures. There are, however, a few issues that will need to be addressed prior to widespread use of this technique, including sensor response non-linearity at saturation and imperfect blackbody conditions.

7.1 Assumptions

In calibrating and measuring events with the three-color technique, certain assumptions have made. These assumptions include the emissivity of the test subjects being analyzed with this technique, the optical density of fireballs, the linear relationship between temperature and color ratios, and atmospheric effects on the results. This section discusses some of the most prominent assumptions made in development and use of the three-color technique.

7.1.1 Emissivity

The emissivity of an object is defined as "the ratio of the radiation emitted by the surface at a given temperature to the radiation emitted by a blackbody at the same temperature [6]." In effect, the emissivity describes how well the surface of interest radiates like a blackbody. In all of the blackbody calculations performed in this research, the emissivity of the objects was assumed to be one, meaning that the objects were assumed to radiate like blackbodies. This assumption was made in order to simplify the calculations, as well as due to the difficulty associated with measuring the emissivity of explosive products.

Real surfaces, including explosive products, do not have constant emissivities. The emissivity of a surface is known to be a function of the surface's

temperature, and the wavelength and direction of the emitted radiation [6]. A surface's emissivity is a complex variable in radiation-based techniques, as it also depends on the condition of the surface (including oxidation, roughness, type of finish, and cleanliness.) Carbon, a common component in explosive products, can have an emissivity ranging from about 0.75 to just over 0.9 [6]. This means that carbon radiates much like a theoretical blackbody. According to Draper et. al, clouds of small particles (soot) will absorb visible light preferentially according to wavelength, while larger particles (coal, char and ash) will absorb visible light equally at all wavelengths (Gray emissivity) [35].

Most radiation-based temperature measurement techniques assume the object to perform as a graybody, where the emissivity is a constant and independent of temperature, wavelength, and direction. For example, Reinhard et. al used high-speed spectroscopy to measure the temperatures of certain test subjects, including Composition B. The spectra captured during the event were fitted to a blackbody equation with the assumption that the test subject has an emissivity of one.

This assumption of graybody characteristics is certainly a source of error in the measurements made with the three-color technique. Further development is needed to identify how much error is attributed to this assumption, as well as when this assumption does not apply.

7.1.2 Optical density of fireballs

As the three-color technique utilizes visible radiation to measure an event's temperature, it can only measure objects that are unconcealed by other objects or gases. Depending on the level of reaction completeness, fireballs can be highly translucent or optically thick. As the fullness of reaction decreases, more of the reactants are left behind, increasing the optical density of the fireball. For lower-quality energetic materials, this will cause errors in the three-color temperature measurements.

Lewis, Rumchik, and Smith found that, early in the explosive event, the spectra of an RDX fireball does, in fact, differ greatly from the spectra collected at the interior of the fireball. As the fireball expands and combustion occurs more evenly throughout the entire fireball volume, the difference in spectra between the interior and exterior locations is negligible [36].

When using the three-color technique to measure the temperatures of an energetic material known to be optically thick, the resulting temperature is attributed to the combustion occurring near the surface of the fireball. If temperatures at the interior of the fireball are needed, a direct line of sight is needed

between the charge surface and the camera without obstruction from fireball particulates.

7.1.3   Linear relationships between temperature and color ratios

In Section 5.1.2, the blackbody calibration process is discussed in detail. Upon determination of the red-to-green, blue-to-green, and blue-to-red color ratios as functions of temperature, a linear fit was applied to the data and used in later tests to measure temperature. In applying a linear fit, the assumption is made that the color ratios are linearly related to temperature past the temperatures at which the tungsten filament was imaged. At the relatively narrow range of filament temperatures, this is an acceptable approximation. However, if the tungsten filament does, in fact, approximate a blackbody well (as it should), this assumption is incorrect. The theoretical color ratios of a blackbody as calculated from Planck's Law are shown in Figure 1.3, repeated here as Figure 7.1. From this plot, it is easily seen that the color ratios are related to temperature exponentially. At the range of temperatures evaluated in this research, a linear fit serves as a good approximation. However, to apply the system to a large range of temperatures (such as 1000-6000 K, as shown here), an exponential fit to the data would be more appropriate.

7.1.4   Atmospheric effects on the results

Another major assumption inherent to the three-color technique, as well as other radiation-based techniques, is the atmosphere's effect on the calculated temperatures. For radiation-based techniques it is important to evaluate radiation intensities in wavelength bands that do not contain spectral peaks. Spectral peaks can cause error in temperature measurement using a radiation-based technique.

The three-color technique assumes that the wavelength bands in which radiation intensity is evaluated do not contain absorption bands from the chemical content of the atmosphere. As the light radiated from the event travels toward the photosensor in the camera, different elements present in the atmosphere can alter the intensity of the radiation by the time it reaches the sensor. Because of this, absorption bands will affect temperature measurements just as spectral peaks do. The assumption that absorption lines are not present in the wavelength bands of interest is not correct, as absorption lines are present throughout the radiation spectrum, including in the red, green, and blue wavelength bands used for the three-color technique. It is assumed, however, that these absorption lines have
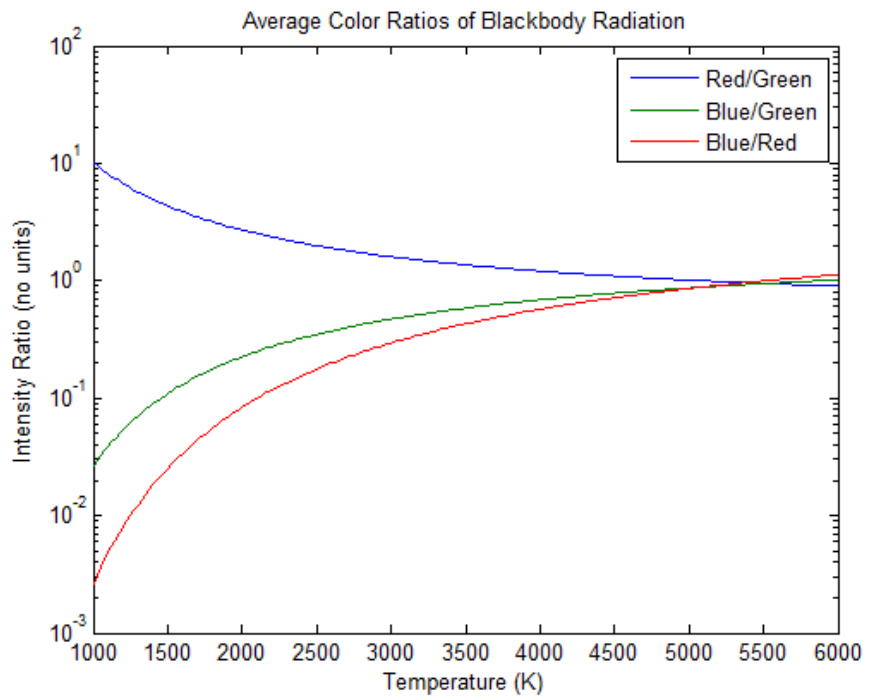
Figure 7.1: Red-to-green, blue-to-green, and blue-to-red color ratios for a black-body as a function of temperature as calculated from Planck's Law.

a negligible effect on the temperature measurements made with the three-color technique.

To understand how greatly these absorption bands affect the three-color technique's results, testing should be performed in a controlled atmosphere where the surrounding gas is known. Introduction of other known atmospheric conditions while imaging the same test subject, would provide insight into how absorption lines affect the resulting temperatures. Further development is needed to identify the errors due to atmospheric composition.

7.2   Limitations of the three-color technique

Because the three-color technique is a relatively new development in the field of temperature measurement, the technique possesses certain limitations. One of the most important limitations of this technique is the inability to measure temperatures during the energetic material reaction. As mentioned in the previous section, this is due to the fireball and products being optically thick, concealing the visible radiation from the event.

In addition, this technique also makes major assumptions that the test subjects behave as blackbodies, possessing constant, unity emissivities and radiating equally at all temperatures and in all directions. As mentioned previously, this is not always an appropriate assumption. To remove this limitation, the blackbody characteristics of each test subject must be known and applied within the calibration and measurement procedures. This characterization is immensely time-consuming and difficult and, therefore, an inherent limitation of the technique.

The three-color technique is also limited in its lower temperature measurement capabilities. At temperatures of less than 1000 K, radiation occurs most prominently in the infrared region. As the camera is designed to measure the photons in the visible region, these lower temperatures cannot be measured accurately.

7.3   Full Imaging System Calibration

For the most accurate results, a tedious calibration of the camera and lens used for a particular experiment is highly recommended. The calibration takes into account various characteristics that are difficult to measure, including the sensor responsivity, bandpass of the color filters, variations in the internal electronics, and losses in the lens. After performing the calibration, any change in the equipment, including use of a different lens, can result in inaccurate results.

Therefore, a full calibration is highly recommended for each imaging set-up (camera and lens.)

For the energetic material testing performed in this research, only the shotgun shell primers used a fully calibrated imaging system (the v611 high-speed camera and a particular lens.) Because the high-speed cameras were all borrowed from various entities (Energetic Material Testing and Research Center (EMRTC) and Sandia National Laboratories), use of the same camera for all three of the tests was difficult. Therefore, some of the errors present in the pyrotechnic and NONEL results are attributed to the lack of full imaging system calibration. Since the published spectral sensitivities of the Phantom v611 (primers) and v710 (pyrotechnics) are the same, it is expected that most of the calibration-related errors are from the small deviations from the published spectral sensitivities and miscellaneous electronic and optical losses throughout the system. No spectral sensitivity data is published for the v7.1, so it is unknown how greatly the lack of calibration affected the NONEL test results. It is important to note, however, that the NONEL differed from published values the most out of the three energetic tests. Because of this, it is expected that the v7.1 utilizes a sensor with a much different response than the v611 and v710.

As shown in Chapter 5, the calibration of the two-color and three-color methods utilize a linear fit to determine the unknown temperature of an object. From Figures 5.4 and 5.9 (reproduced for reference purposes in Figures 7.2 and 7.3), it is clear that the linear fit is a good approximation of the relationships between intensity ratio and temperature. Despite this, the use of a linear fit in these methods introduces nontrivial errors.

Figure 7.4 shows the temperatures measured from the tungsten bulb calibration data without ambient lighting using the two-color method. While this calculation seems irrelevant because of the circular process of measuring temperatures in the calibration data with the results obtained from the same data, this process performs two key tasks. First, performing the calculations on the original calibration data supports the validity of the calculations and boosts confidence in the results. Second, this check allows for the linear fit errors inherent to the two- and three-color methods to be observed.

In Figure 7.4, the individual datum points are the temperatures measured from each sequential spectrum, while the solid lines indicate the theoretical temperature of the filament according to the voltage and current settings at that time. Clearly, the average of the points agrees well with the theoretical values at each of the various power levels. From this plot, it is estimated that the linear fit in the two-color method and the averaging of the wavelength ranges (10 nm wide bands) introduces an uncertainty of approximately ± 20 K. To reduce this error as much as possible, it is recommended that many sets of spectra be taken at various temperatures to increase the repeatability of each measurement. During this
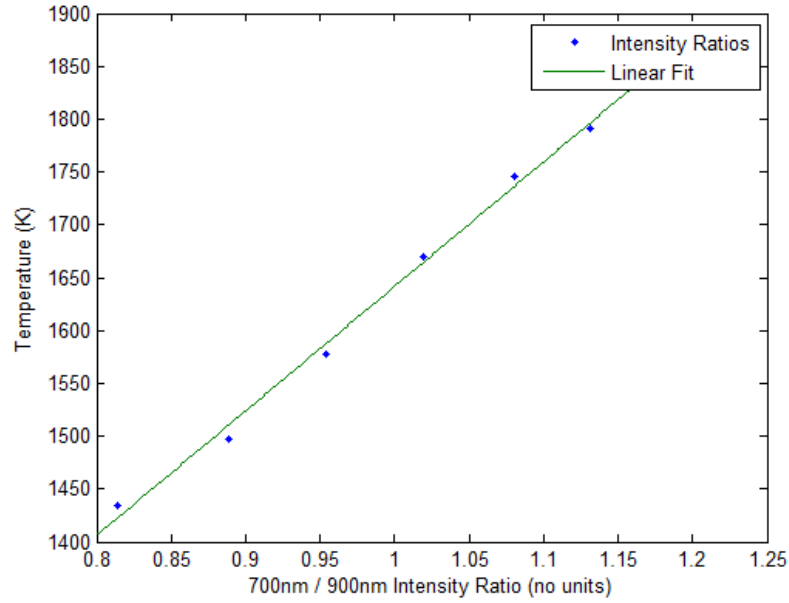
Figure 7.2: Tungsten bulb calibration curve from 700-to-900-nm intensity ratios.
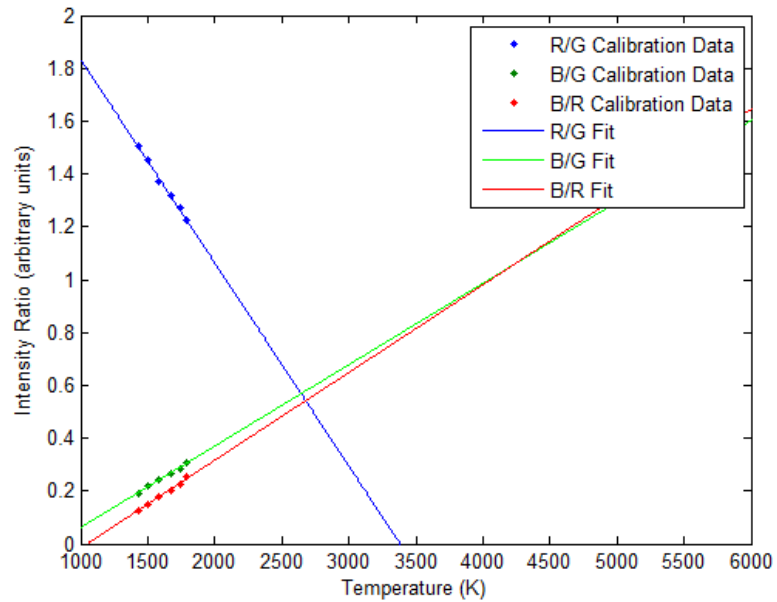
Figure 7.3: The full calibration fit for the Phantom v611, calculated from the right side of Equation 5.4. The linear fit seen here is used in future tests to measure temperature.

Figure 7.4: Comparison between two-color-measured and theoretical filament temperatures at various power levels. The solid lines indicate the theoretical filament temperature as calculated from the voltage and current settings.

calibration, only 20 spectra were collected at each filament temperature. A larger number of spectral samples would reduce the effects of anomalies in the data and minimize this error.

Figure 7.5 shows the errors measured using the three-color method on the original tungsten bulb data. The uncertainty of the three-color method as related to the linear fit is approximately ± 70 K. This larger uncertainty is attributed to the larger presence of noise in the Phantom's response. A larger, but not excessive, response variation is observed in the Phantom as opposed to the spectrometer. This is attributed to the differences in design intent between the spectrometer and the Phantom. The spectrometer is designed for accurately measuring radiation across a broad spectrum, while the Phantom is designed for measuring radiation in certain wavelength bands with sufficient accuracy to reproduce the physical scene.

7.4   Use of Tungsten Bulb as a Blackbody

While the Pasco Scientific TD-8555 tungsten halogen bulb serves as a good approximation of a blackbody for educational purposes, it is not a radiometric

Figure 7.5: Comparison between three-color-measured and theoretical filament temperatures at various power levels. The solid lines indicate the theoretical filament temperature as calculated from the voltage and current settings.

calibration standard. This means that the tungsten bulb is not designed specifically for calibration of a system to a blackbody, and, therefore, its blackbody correctness is not necessarily highly reliable. It is recommended that, if the three-color system is to be used for temperature measurement during an experiment, the calibration accuracy of a true radiometric standard should be compared to the tungsten bulb to determine if the TD-8555 is sufficient. It is possible that the improvement gained with the much more expensive radiometric standard is well worth the cost, but it is also possible that the educational-quality tungsten halogen bulb is the most cost effective blackbody available. Examples of radiometric calibration standards used by other sources are the Omega Engineering BB-4A [22] and Ocean Optics LS-1-CAL sources [3].

7.5 Presence of Ambient Light

As the foundation of the three-color temperature measurement technique is the radiated energy from high temperature sources, the presence of other radiation sources is clearly a source of error. Any ambient lighting, including incandescent and fluorescent light sources, will affect the level of radiation measured by any spectrometer or camera. In the energetic material tests, only the

pyrotechnic tests were performed with normal levels of ambient light. This ambient light, while low due to testing in a unlit fume hood, was allowed for safe initiation and monitoring of the mixture during the reaction. Therefore, ambient lighting is a source of error for the pyrotechnic test results. The other two test subjects, shotgun shell primers and NONEL shock tube, were performed with minimal ambient lighting. For future use of the three-color technique, it is highly recommended that ambient lighting is limited during data collection. For large-scale tests, however, this is a nearly impossible task necessitating the need for an alternative solution. For tests that must be performed with ambient lighting, background correction is recommended. Figure 7.6 shows the effects of ambient lighting on data without having calibrated the system to the particular ambient lighting conditions. This plot shows the results of tungsten bulb data acquired with ambient lighting as evaluated with the linear fit for the data without ambient lighting. As mentioned earlier, approximately ±70 K of the error is attributed to the linear fit used in the system calibration. From this plot, an error of about ±80 K is seen, meaning that ±10 K is attributed to the lack of the correct ambient lighting calibration. As discussed in Section 5.1.3, the effects of ambient lighting are more noticeable at lower temperatures, but become negligible at the higher temperatures. At the temperatures evaluated here (1400-1800 K), the error is only ±10 K at most.
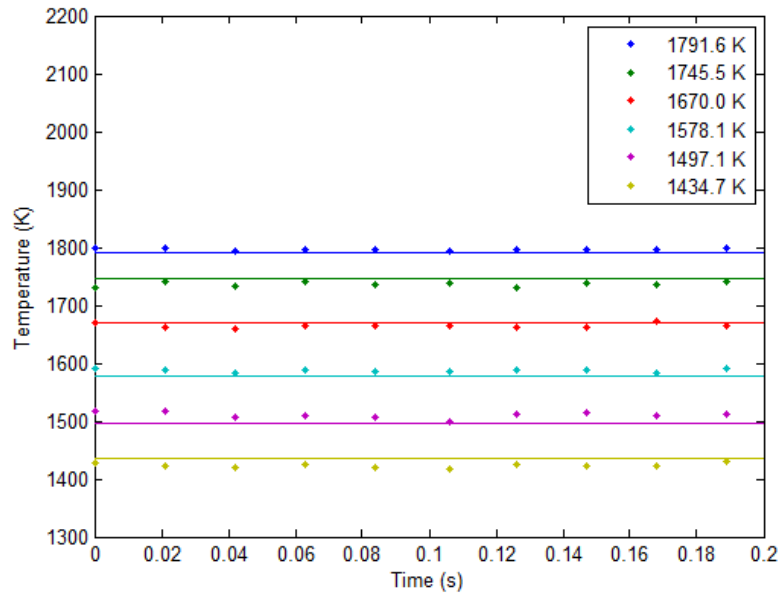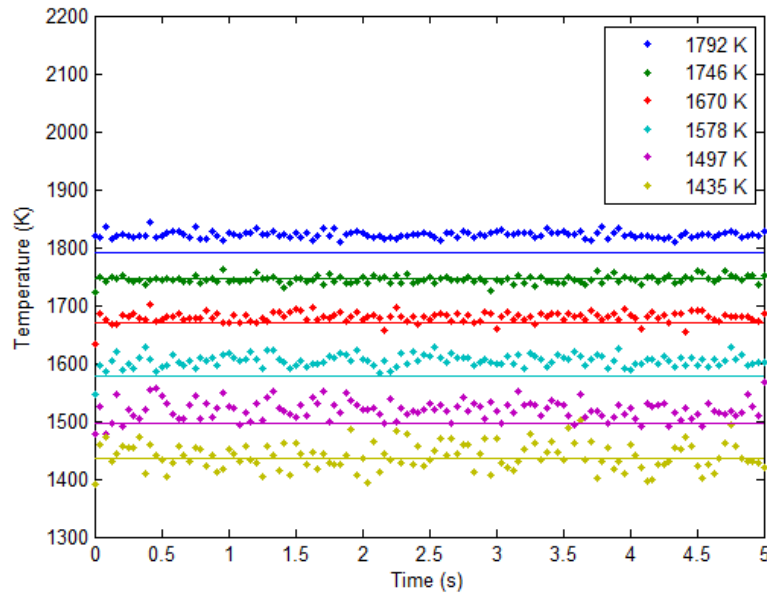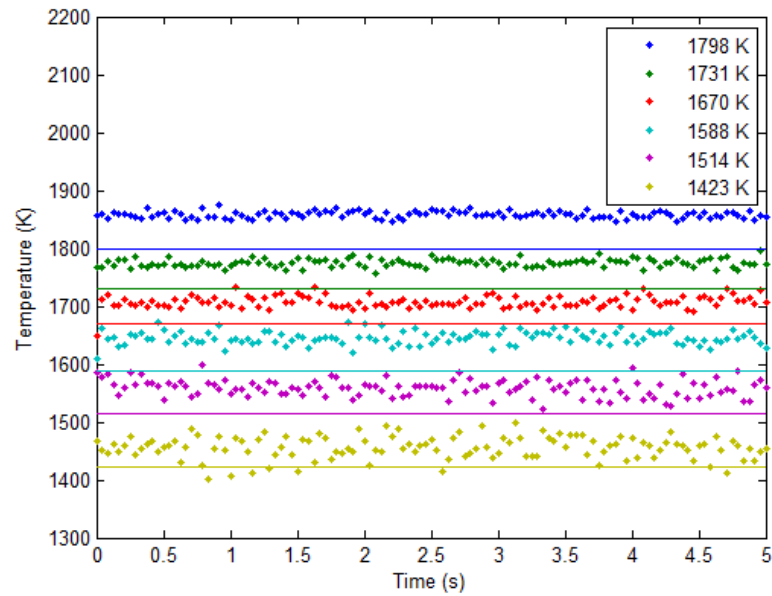
Figure 7.6: Comparison between three-color-measured and theoretical filament temperatures at various power levels. The solid lines indicate the theoretical filament temperature as calculated from the voltage and current settings. The errors in this plot are from both the linear fit and the presence of ambient lighting for which the system has not been calibrated.

7.6 Non-linearity of Sensor Response at Saturation

An inherent issue involved with evaluating optical data is the possibility of pixel saturation. The pixels of a CFA collect light input for the amount of time that the shutter is open. If care is not taken to avoid it, the shutter speed might allow so much light to enter the camera that the actual light level surpasses the maximum intensity level that can be measured by the camera. If this occurs, those pixels are said to be "saturated," and the camera will output inaccurate intensity values, which are the maximum intensities determined by the bit depth of the camera (i.e. 255 for the Phantom v611). To avoid saturation of the pixels, very low light input was allowed into the cameras during calibration and testing–just enough for the maximum intensity values to be measured without reaching the maximum measureable intensity. The surroundings in these tests were, therefore, not visible in the data, as they did not output/reflect light at an intensity level near the tungsten bulb.

To circumvent this issue in future use of the three-color technique as applied to energetic materials, a process of trial-and-error is recommended. To determine the exposure and lens settings needed for a particular test subject, the test subject needs to be at the maximum brightness it will achieve in the event. Therefore, preliminary shots need to be made to fine-tune the exposure and lens settings for maximum response without saturation. Development of a library of test subjects and successful exposure/lens settings could provide starting values for the settings from which to begin tuning the system. For test subjects that can be at maximum brightness for sufficient time (such as the tungsten filament bulb), tuning of the exposure and lens settings is a much easier task.

7.7 Non-blackbody Characteristics of the Test Subjects

Use of the three-color temperature measurement technique implies that the test subjects behave as blackbodies, with perfect emission and perfect absorption of radiation. It has been noted by various sources that this is not always an appropriate assumption. In tests of Detasheet-C, Lebel et. al noted that blackbody-type radiation was, in fact, observed because the spectra could be fitted to Planck's Law. This close resemblance to blackbody behavior is attributed to the material being fuel-rich. They explain that blackbody radiation in a flame is typically from particulates of carbonaceous soot, while fuel-lean materials produce radiation corresponding to the excitation peaks of radical intermediates [3]. In future application of the three-color temperature measurement technique, spectra should be collected during each test to ensure that the spectra

indicate blackbody radiation by fitting well to Planck's Law. Further research is needed for test subjects that do not behave like blackbodies.

CHAPTER 8

CONCLUSIONS

In conclusion, the three-color temperature measurement technique has been applied successfully to new energetic material events, including shotgun shell primers, pyrotechnic mixtures, and NONEL shock tube. This technique answers many issues present in conventional techniques. Because it does not need contact with the subject, the sensor is capable of measuring extreme temperatures without incurring damage. In addition, the technique uses radiation captured in the form of images–therefore, providing spatially-resolved temperature that is not available with any other technique. The technique is also fast enough to temporally-resolve energetic material events–the response is limited by the frame rate of the camera.

To provide temperatures with which to compare those measured by the three-color technique, spectrometry-based techniques were employed. Two techniques were used–the first of which, known as two-color pyrometry, used the color intensity ratios in two specific wavelength bands. The second spectrometry technique fits Planck's Law to measured spectra and calculates the temperature from the fit constants. These techniques were shown to agree well with each other and with the three-color technique in most instances.

MATLAB code was developed to decompose raw Phantom cine files into their respective frames and separate these frames into the pixels filtered by red, green, and blue wavelengths. The MATLAB codes enabled initial calibration of the system to an approximate blackbody, as well as temperature calculation of each pixel's temperature using the surrounding pixel values.

Finally, areas for improvement and sources of error in the three-color technique were presented. Some of the most prevalent limitations of this technique include measuring only the surface temperatures of optically-thick fireballs as well as the problems associated with treating the test subjects as blackbodies. The technique promises to be a useful tool in the energetic materials field, as it alleviates many issues present in conventional techniques. Before full application of the three-color technique, however, the imaging system must be fully calibrated and the test subject must behave like a blackbody for maximum accuracy.

REFERENCES

[1] Gruner, K. D., 2003. Principles of non-contact temperature measurement, December.

[2] Hopkins, M., Alastair, T., and Neville, M., 1988. "Development of explosive monitoring techniques for use in quality control and production blast analysis". In Proc. Explosives in Mining Workshop, Melbourne, Vic., Australia, pp. 39–43.

[3] Lebel, L., Brousseau, P., Erhardt, L., and Andrews, W., 2013. "Measurements of the temperature inside an explosive fireball". *Journal of Applied Mechanics,* **80**, pp. 031702–1–031702–6.

[4] Cavanough, G., and Onederra, I., 2011. "Development of pressure and temperature gauges to monitor in situ performance of commercial explosives". *Mining Technology,* **120**, pp. 74–79.

[5] Sutton, G. P., and Biblarz, O., 2001. *Rocket Propulsion Elements*. John Wiley & Sons.

[6] Cengel, Y. A., and Ghajar, A. J., 2011. *Heat and Mass Transfer, Fundamentals and Applications*, 4th ed. McGraw-Hill.

[7] Stone, M. C., 2003. *A Field Guide to Digital Color*. A K Peters, Limited. ebrary.

[8] Gunturk, B. K., Glotzbach, J., Altunbasak, Y., Schafer, R. W., and Mersereau, R. M., 2005. "Demosaicking: Color filter array interpolation". *IEEE Signal Processing Magazine,* **22**, January, pp. 44–54.

[9] Hirakawa, K., and Wolfe, P. J. A novel color filter array design scheme significantly reduces hardware complexity.

[10] Smilowitz, L., Henson, B., Sandstrom, M., Asay, B., Oschwalk, D., Romero, J., and Novak, A., 2005. "Fast internal temperature measurements in pbx9501 thermal explosions". *Shock Compression of Condensed Matter,* **845**, pp. 1211–1214.

[11] Simpson, R., 1999. Unraveling the mystery of detonation. webpage, June.

[12] Lewis, W. K., and Rumchik, C. G., 2009. "Measurement of apparent temperature in post-detonation fireballs using atomic emission spectroscopy". *Journal of Applied Physics,* **105**, pp. 0561041–0561043.

[13] Wehrmeyer, J. A., Osborne, R. J., and Trinh, H. P., 2003. "Measuring rocket engine temperature with hydrogen raman spectroscopy". In Temperature: Its Measurement and Control in Science and Industry, D. C. Ripple, ed., Vol. 7, American Institute of Physics, pp. 837–842.

[14] Strand, L. D., Cohen, N. S., Jones, M. D., and Ray, R. L., 1994. Characterization of hybrid rocket internal heat flux and htpb fuel pyrolysis. Tech. rep., Jet Propulsion Laboratory.

[15] Chiaverini, M. J., 1997. "Regression rate and pyrolysis behavior of htpb-based solid fuels in a hybrid rocket motor". PhD thesis, Pennsylvania State University.

[16] Hargather, M. J., 2012. Background-oriented schlieren diagnostics for large-scale explosive testing. Received from M. Hargather Sept. 17, 2012., April.

[17] Fu, T., Wang, Z., and Cheng, X., 2010. "Temperature measurements of diesel fuel combustion with multicolor pyrometry". *Journal of Heat Transfer,* **132**, May, pp. 0516021–0516027.

[18] Tarasov, M., Karpenko, I., Sudovtsov, V., and Tolshmyakov, A., 2007. "Measuring the brightness temperature of a detonation front in a porous explosive". *Combustion, Explosion, and Shock Waves,* **43**(4), pp. 465–467.

[19] Childs, P. R. N., Greenwood, J. R., and Long, C. A., 2000. "Review of temperature measurement". *Review of Scientific Instruments,* **71**, pp. 2959–2978.

[20] Panditrao, A., and Rege, P., 2009. *Advances in Numerical Methods, Lecture Notes in Electrical Engineering*, Vol. 11. Springer Science+Business Media, ch. Visible light source temperature estimation using digital camera photography, pp. 249–258.

[21] Panditrao, A. M., and Rege, P. P., 2009. Estimation of furnace temperature distribution using digital photographic images. Tech. rep., Cummins College of Engineering.

[22] Densmore, J., Biss, M., McNesby, K., and Homan, B., 2011. "High-speed digital color imaging pyrometry". *Applied Optics,* **50**(17), pp. 2659–2665.

[23] Toshiba, 2004. Toshiba ccd linear image sensor: Tcd1304dg. Online specification sheet, January.

[24] Vision-Research. Color & spectral response curve (vseries).

[25] Galang, J., 2010. The danger of green laser pointers, August.

[26] Nave, R. Sodium spectrum.

[27] Newport. 1000 watt xenon arc lamp (ozone free).

[28] , 2013. Graph suchi yomitori system, September.

[29] DynoNobel. About us: History.

[30] Densmore, J. M., Homan, B. E., Biss, M. M., and McNesby, K. L., 2011. "High-speed two-camera imaging pyrometer for mapping fireball temperatures". *Applied Optics,* **50**(33), November, pp. 6267–6271.

[31] De Yong, L., 1985. An evaluation of temperature and heat flux of gasless and gassy percussion primers. Tech. Rep. MRL-R-971, Australian Department of Defence, August.

[32] Kelly, M., 1967. "A radiant energy technique to measure explosive output". In Fifth Symposium on Electroexplosive Devices, The Franklin Institute, pp. 1–12.1–1–12.36.

[33] Hegde, G., Pathak, A., Jagadeesh, G., Oommen, C., Arunan, E., and Reddy, K., 2004. Spectroscopic studies of micro-explosions. Referenced by Suriyanarayanan et al. in Quantitative Characterization of the Flow Field of A Micro-Explosion Using Background Oriented Schlieren.

[34] DaBin, L., 2002. "Study of the initiation, explosion transfering and output character of nonel tube". PhD thesis, Nanjing University of Technology and Engineering.

[35] Draper, T. S., Zeltner, D., Tree, D. R., Xue, Y., and Tsiava, R., 2012. "Two-dimensional flame temperature and emissivity measurements of pulverized oxy-coal flames". *Applied Energy,* **95**, pp. 38–44.

[36] Lewis, W. K., Rumchik, C. G., and Smith, M. J., 2013. "Emission spectroscopy of the interior of optically dense post-detonation fireballs". *Journal of Applied Physics,* **113**, pp. 024903–1–024903–4.

APPENDIX A

MATLAB CODE: RAW CINE FILE DECOMPOSITION INTO TIFF IMAGE FILES

The following code uses the Vision Research Software Development Kit (SDK) to decompose a RAW cine into its respective tiff images without performing demosaicking. All rights belong to Vision Research, Inc.

```matlab
% Raw Phantom cine decomposition into raw tiffs
% Author: Megan Tribble and Vision Research, Inc.
% Last revised: 03/04/2014
clear all
clc
warning('off','all');
LoadPhantomLibraries();
RegisterPhantom(true);
showImage = false;

%% Create the cine handle from the cine file.
[FileName,PathName,FilterIndex] = uigetfile('C:\Users\Megan ...
    Tribble\Documents\NMT\- ...
    GraduateStudy\Thesis\RAWtoRGB\CineDecomposition\*.cine',    ...
    'Locate the cine file.');
CinePath = strcat(PathName,FileName);
Dialog = inputdlg('Folder Date (YYYYMMDD)','User Input', [1 60]);
[HRES, cineHandle] = PhNewCineFromFile(CinePath);
if (HRES<0)
    [message] = PhGetErrorMessage( HRES );
    error(['Cine handle creation error: ' message]);
end

%% Get information about cine
%read the saved range
pCFA = libpointer('uint32Ptr',0);
PhGetCineInfo(cineHandle, PhFileConst.GCI_CFA, pCFA);
CFA = pCFA.Value;
pFirstIm = libpointer('int32Ptr',0);
PhGetCineInfo(cineHandle, PhFileConst.GCI_FIRSTIMAGENO, pFirstIm);
firstIm = pFirstIm.Value;
```

```matlab
29 pImCount = libpointer('uint32Ptr',0);
30 PhGetCineInfo(cineHandle, PhFileConst.GCI_IMAGECOUNT, pImCount);
31 lastIm = int32(double(firstIm) + double(pImCount.Value) - 1);
32 %get cine image buffer size
33 pInfVal = libpointer('uint32Ptr',0);
34 PhGetCineInfo(cineHandle, PhFileConst.GCI_MAXIMGSIZE, pInfVal);
35 imgSizeInBytes = pInfVal.Value;
36 %The image flip for GetCineImage function is inhibited.
37 pInfVal = libpointer('int32Ptr',false);
38 PhSetCineInfo(cineHandle, PhFileConst.GCI_VFLIPVIEWACTIVE, pInfVal);
39 %Create the image range to be read
40 imgRange = get(libstruct('tagIMRANGE'));
41 A = char(strcat('C:\Users\Megan Tribble\Documents\NMT\- ...
      GraduateStudy\Thesis\RAWtoRGB\CineDecomposition\CineImages_', ...
      Dialog(1)));
42 mkdir(A);
43 k = 1;
44 for i = firstIm:1:lastIm
45     %take one image at imageNo
46     imgRange.First = i;
47     imgRange.Cnt = 1;
48
49     %% Read the cine image into the buffer
50     pVal = libpointer('uint32Ptr',6); % No demosaicing
51     PhSetCineInfo(cineHandle, PhFileConst.GCI_INTALGO,pVal);
52     [HRES, unshiftedIm, imgHeader] = PhGetCineImage(cineHandle, ...
          imgRange, imgSizeInBytes);
53     % Read image information from header
54     isColorImage = IsColorHeader(imgHeader);
55     is16bppImage = Is16BitHeader(imgHeader);
56
57     %% Transform 1D image pixels to 1D/3D image pixels to be ...
          used with MATLAB
58     if (HRES >= 0)
59         [unshiftedIm] = ...
              ExtractImageMatrixFromImageBuffer(unshiftedIm, ...
              imgHeader);
60         if (isColorImage)
61             samplespp = 3;
62         else
63             samplespp = 1;
64         end
65         bps = GetEffectiveBitsFromIH(imgHeader);
66         [matlabIm, unshiftedIm] = ...
              ConstructMatlabImage(unshiftedIm, imgHeader.biWidth, ...
              imgHeader.biHeight, samplespp, bps);
67     end
68     Name = char(strcat('C:\Users\Megan Tribble\Documents\NMT\- ...
          GraduateStudy\Thesis\RAWtoRGB\CineDecomposition\  ...
          CineImages_',Dialog(1),'\',num2str(k),'.tiff'));
```

```
69      imwrite(matlabIm,Name);
70      k = k+1;
71  end
72  UnregisterPhantom();
73  UnloadPhantomLibraries();
```

APPENDIX B

MATLAB CODE: CALIBRATION FUNCTION

This code takes the color ratios seen at various known temperatures and produces a calibration curve based off of Equation 5.4.

```matlab
1  clear all
2  clc
3  %% Variables for Planck's Law
4  Emissivity = 1;
5  C1 = 37413*10^(-20); % W/m^2
6  C2 = 14387.8*10^(-6); % m-K
7  % lambda = (392:3.15:700)*10^(-9); % m Phantom
8  lambda = (390:4.9:700)*10^(-9); % m Nikon
9  %% Read in calibration data
10 Phantom = csvread('PhantomSensitivities_RGB.csv'); % Spectral ...
       sensitivity curve for Phantom (RedL|Red|GreenL|Green|BlueL|Blue)
11 BBCal = csvread('BBCal_20140307_Set2_VersA.csv'); % Phantom BB ...
       calibration (Temp|R/G|B/G|B/R)
12 CalRG = zeros(length(BBCal),1);      RGRatio = ...
       zeros(length(BBCal),1);
13 CalBG = zeros(length(BBCal),1);      BGRatio = ...
       zeros(length(BBCal),1);
14 CalBR = zeros(length(BBCal),1);      BRRatio = ...
       zeros(length(BBCal),1);
15 %% Calculate calibration factor curves for Phantom
16 for i = 1:length(BBCal)
17     T = BBCal(i,1);    % Kelvin
18     BBRG = BBCal(i,2);
19     BBBG = BBCal(i,3);
20     BBBR = BBCal(i,4);
21     % Blackbody curve
22     SpectralRadiance = ...
           transpose(Emissivity*(C1./(lambda.^5)).*(1./(exp(C2./   ...
           (lambda.*T))-1)));
23     % Product of spectral sensitivity and blackbody curve
24     RedProduct = SpectralRadiance.*Phantom(:,2);
25     GreenProduct = SpectralRadiance.*Phantom(:,4);
26     BlueProduct = SpectralRadiance.*Phantom(:,6);
27     % Take integral of product curve
```

```matlab
28      RedIntegral = trapz(lambda,RedProduct);
29      GreenIntegral = trapz(lambda,GreenProduct);
30      BlueIntegral = trapz(lambda,BlueProduct);
31      % Solve for calibration factors
32      CalRG(i,1) = BBRG*(GreenIntegral/RedIntegral);
33      CalBG(i,1) = BBBG*(GreenIntegral/BlueIntegral);
34      CalBR(i,1) = BBBR*(RedIntegral/BlueIntegral);
35      RGRatio(i,1) = CalRG(i,1)*(RedIntegral/GreenIntegral);
36      BGRatio(i,1) = CalBG(i,1)*(BlueIntegral/GreenIntegral);
37      BRRatio(i,1) = CalBR(i,1)*(BlueIntegral/RedIntegral);
38  end
39
40  Ratios = 0:0.001:5;
41  RGCoeff = polyfit(RGRatio(:,1),BBCal(:,1),1);
42  BGCoeff = polyfit(BGRatio(:,1),BBCal(:,1),1);
43  BRCoeff = polyfit(BRRatio(:,1),BBCal(:,1),1);
44  RGTemp = polyval(RGCoeff,Ratios);
45  BGTemp = polyval(BGCoeff,Ratios);
46  BRTemp = polyval(BRCoeff,Ratios);
47  plot(RGRatio(:,1),BBCal(:,1),'.',BGRatio(:,1),BBCal(:,1),'.',    ...
        BRRatio(:,1),BBCal(:,1),'.',Ratios,RGTemp,Ratios,BGTemp,    ...
        Ratios,BRTemp)
48  ylim([1000 6000])
49  legend('R/G Calibration Data','B/G Calibration Data','B/R ...
        Calibration Data','R/G Fit','B/G Fit','B/R Fit')
50  xlabel('Temperature (K)')
51  ylabel('Intensity Ratio (arbitrary units)')
52  title('Calibrated Relationship of Intensity Ratio vs. Temperature')
```

APPENDIX C

MATLAB CODE: TIFF RGB SEPARATION AND PROCESSING (CROPPING)

This code converts the raw tiff files from the high speed video into temperature videos and plots the average temperature in the cropped region with respect to time.

```matlab
1  % ─────────────────────────────────────────
2  % Convert directory of tiff images into temperature video and ...
       history plot
3  % Author:           Megan Tribble (New Mexico Tech)
4  % Last Revision:    04/19/14
5  % *sort_nat MUST BE ACCESSIBLE TO MATLAB*
6  % ─────────────────────────────────────────
7  clear all
8  clc
9
10 RGCoeff = [-1.2997E+03 3.3823E+03];
11 BGCoeff = [3.2479E+03 800.8742];
12 BRCoeff = [3.0108E+03 1.0507E+03];
13 %% Locate tiff files to process and gather necessary information
14 Images = uigetdir('C:\Users\Megan Tribble\Documents\NMT\- ...
       GraduateStudy\Thesis\Data','Locate the directory containing ...
       the tiff files to process.');
15 DataInfo = inputdlg({'Folder Date (YYYYMMDD)','Test ...
       Subject','Test No.','Frame Rate (fps)'},'User Input', [1 60]);
16 button = questdlg('Create temperature video?','User input needed');
17 warning off Images:initSize:adjustingMag
18 files = dir(strcat(Images,'\*.tiff'));
19 FileStructures = struct2cell(files);
20 [SortedFiles,index] = sort_nat(FileStructures(1,:));
21 %%
22 mov = avifile(char(strcat(DataInfo(1),'_',DataInfo(2),          ...
       DataInfo(3),'.avi')),'fps',2,'compression','None');
23 for z = 1:50:2015
24     warning off MATLAB:tifflib:TIFFReadDirectory:libraryWarning
25     Tiff = double(imread(SortedFiles{z}));
26     %% User-defined cropping for first image, repeat dimensions ...
```

```matlab
                afterward
27      TiffIm = Tiff/max(max(Tiff)); % Normalize first *displayed* ...
            image for easy cropping
28      if z == 1
29          crop1 = imcrop(TiffIm);
30          t = inputdlg('Enter crop dimensions:', 'User Input', [1 ...
                50]);
31          data = ceil(str2num(t{:}));
32      end
33      %%  Calculate average red, green, and blue in 3x3 matrix ...
            based on even/odd indices
34      for i = 1:1:size(Tiff,1)-2        % rows
35          for j = 1:1:size(Tiff,2)-2    % columns
36              if (mod(i,2) ~= 0) && (mod(j,2) ~= 0)
37                  % Type 1
38                  AvgRed1 = ((Tiff(i+1,j)+Tiff(i+1,j+2))/2);
39                  AvgGreen1 = ((Tiff(i,j)+Tiff(i,j+2)+      ...
                        Tiff(i+1,j+1)+Tiff(i+2,j)+Tiff(i+2,j+2))/5);
40                  AvgBlue1 = ((Tiff(i,j+1)+Tiff(i+2,j+1))/2);
41              elseif (mod(i,2) ~= 0) && (mod(j,2) == 0)
42                  % Type 2
43                  AvgRed1 = Tiff(i+1,j+1);
44                  AvgGreen1 = ((Tiff(i,j+1)+Tiff(i+1,j)+     ...
                        Tiff(i+1,j+2)+Tiff(i+2,j+1))/4);
45                  AvgBlue1 = ((Tiff(i,j)+Tiff(i,j+2)+      ...
                        Tiff(i+2,j)+Tiff(i+2,j+2))/4);
46              elseif (mod(i,2) == 0) && (mod(j,2) ~= 0)
47                  % Type 3
48                  AvgRed1 = ((Tiff(i,j)+Tiff(i,j+2)+      ...
                        Tiff(i+2,j)+Tiff(i+2,j+2))/4);
49                  AvgGreen1 = ((Tiff(i,j+1)+Tiff(i+1,j)+     ...
                        Tiff(i+1,j+2)+Tiff(i+2,j+1))/4);
50                  AvgBlue1 = Tiff(i+1,j+1);
51              else %(mod(i,2) == 0) && (mod(j,2) == 0)
52                  % Type 4
53                  AvgRed1 = ((Tiff(i,j+1)+Tiff(i+2,j+1))/2);
54                  AvgGreen1 = ((Tiff(i,j)+Tiff(i,j+2)+     ...
                        Tiff(i+1,j+1)+Tiff(i+2,j)+Tiff(i+2,j+2))/5);
55                  AvgBlue1 = ((Tiff(i+1,j)+Tiff(i+1,j+2))/2);
56              end
57              RG1 = AvgRed1/AvgGreen1;
58              BG1 = AvgBlue1/AvgGreen1;
59              BR1 = AvgBlue1/AvgRed1;
60              RGTemp(z) = polyval(RGCoeff,RG1);
61              BGTemp(z) = polyval(BGCoeff,BG1);
62              BRTemp(z) = polyval(BRCoeff,BR1);
63              AverageTemp(z) = (RGTemp(z)+BGTemp(z)+BRTemp(z))/3;
64              TempTiff(i+1,j+1) = AverageTemp(z);
65          end
66      end
```

```matlab
67        RegionTemp(z) = mean2(TempTiff(data(2):(data(2)+data(4)-1), ...
                data(1):(data(1)+(data(3)-1))));
68        Time(z) = (z-1)*(1/str2num(cell2mat(DataInfo(4))));
69        if strcmp(button,'Yes')
70            %% Temperature video creation
71            subplot(1,2,1)
72            imshow(SortedFiles{z+2015})
73            title('Color Image')
74            A = get(gca,'Position');
75            set(gca,'Position',[0.05 0.05 A(3) A(4)])
76            subplot(1,2,2)
77            TiffIm1 = imagesc(TempTiff,[1500 3000]);
78            colormap(hot);
79            axis off
80            h = colorbar;
81            ylabel(h,'Temperature (K)')
82 %            title(strcat(DataInfo(2),' Temperatures',' - Test ...
       ',DataInfo(3),' (',DataInfo(1),'): ',num2str(Time(z)),' s'))
83            title(strcat(' Temperatures at: ',num2str(Time(z)),' s'))
84            set(gca,'Position',[0.1+A(3) 0.25 A(3) A(4)/2])
85            axis equal
86            whitebg('w')
87            drawnow;
88            frame = getframe(gcf);
89            mov = addframe(mov,frame);
90        else strcmp(button,'No')
91            % No video
92        end
93 end
94 AvgTempOverall = mean2(RegionTemp);
95 figure
96 plot(Time,RegionTemp,'.')
97 title(strcat(DataInfo(2),' Temperature History',' - Test ...
       ',DataInfo(3),' (',DataInfo(1),')'))
98 xlabel('Time (seconds)')
99 ylabel('Temperature (K)')
100 if strcmp(button,'Yes');
101 %      mov = movie2avi(G,char(strcat(DataInfo(1),'_',DataInfo(2), ...
           DataInfo(3),'.avi')),'fps',10,'compression','None');
102     mov = close(mov);
103 else
104     % No video
105 end
```

APPENDIX D

MATLAB CODE: VISIBLE SPECTRUM BLACKBODY FIT METHOD

This code determines the temperature with respect to time using the visible spectrum blackbody fit method and the test and background spectra csv files.

```matlab
% ——————————————————————
% Calculate temperature using blackbody fitting method from spectra
% Author:          Megan Tribble (New Mexico Tech)
% Last Revision:   04/28/14
% ——————————————————————
clear all
clc
C1 = 3.74177*10^-16; % W*m^2
C2 = 1.43878*10^-2;  % m*K
%% Locating and reading calibration, test spectra, and ...
    background spectra files
Tungsten = ...
    importdata('SpectrometerResponse_Data1_1791.64K.csv',',');
SpecRes = importdata('CCS200_Responsivity.csv');
[SpectraFileName,SpectraPathName] = uigetfile('*.csv','Select ...
    the spectrometer data file');
TestSpectra = ...
    importdata(strcat(SpectraPathName,SpectraFileName),',');
button = questdlg('Is background correction spectra ...
    available?','User input needed');
if strcmp(button,'Yes')
    [BGSpectraFileName,BGSpectraPathName] = ...
        uigetfile('*.csv','Select the spectrometer backround ...
        data file');
    BGSpectra = ...
        importdata(strcat(BGSpectraPathName,BGSpectraFileName),',');
else strcmp(button,'No')
    BGSpectra = zeros(size(TestSpectra,1),2);
end
Time = TestSpectra(1,2:end)*10^(-3);    % time vector in seconds
%% Responsivity and background correction
ResFitCoeff = polyfit(SpecRes(:,1),SpecRes(:,2),6); % ...
    responsivity of spec as f(wavelength)
```

```matlab
25  TheorTemp = 1791.64;
26  for column = 2:size(TestSpectra,2)
27      for row = 2:size(TestSpectra,1)
28          AvgBGSpectra(row,1) = mean2(BGSpectra(row,2:end));
29          BGCorrSpectra(row,column) = ...
                TestSpectra(row,column)−AvgBGSpectra(row,1);
30          ResCorrSpectra(row,column) = BGCorrSpectra(row,column)/ ...
                  polyval(ResFitCoeff,TestSpectra(row,1));
31          AvgWSpectra(row,1) = mean2(Tungsten(row,2:end));
32          ResCorrWSpectra(row,1) = ...
                AvgWSpectra(row,1)/polyval(ResFitCoeff,Tungsten(row,1));
33          Planck(row,1) = C1/((TestSpectra(row,1)*10^(−9))^5*     ...
                (exp(C2/((TestSpectra(row,1)*10^(−9))*TheorTemp))−1));
34          Sensitivity(row,1) = Planck(row,1)/ResCorrWSpectra(row,1);
35          CALSpectra(row,column) = ...
                ResCorrSpectra(row,column)*Sensitivity(row,1);
36      end
37  end
38  %% Fitting the spectra of interest to the blackbody curve shape
39  for T = 2:size(CALSpectra,2)
40      %% Multiply test spectra by B/I vector to calibrate for spec ...
            response
41      x = TestSpectra(1433:3362,1)*10^(−9); % 500−950 nm: 1433:3362
42      y = CALSpectra(1433:3362,T);
43      modelFun = @(b,x) (b(1)./x.^5).*(1./(exp(b(2)./x)−1));
44      start = [0.00000000000001 0.000009]; %[0.0003; 0.000005];
45      [bFit,r,J,Sigma,mse] = nlinfit(x,y,modelFun,start);
46      [yFit,delta] = nlpredci(modelFun,x,bFit,r,'cov',Sigma);
47      %%
48      PlotW = x*10^9;
49      plot(PlotW,y,'g.',PlotW,yFit,'k−');
50      label = strcat('Fitted Planck equation (C1 ...
            =',num2str(bFit(1)),', C2 =',num2str(bFit(2)),')');
51      legend({'Blackbody calibrated spectrum', ...
            label},'location','SouthEast');
52      xlabel('Wavelength (nm)'); ylabel('Intensity (arbitrary ...
            units)');
53      xlim([min(PlotW) max(PlotW)])
54      Temp(T−1) = C2/bFit(2);
55  end
56
57  figure
58  plot(Time,Temp,'.−')
59  xlim([0 max(Time)])
60  ylim([0 5000])
61  xlabel('Time (s)')
62  ylabel('Temperature (K)')
```